Nikhef-2016-039
SI-HEP-2016-28
QFET-2016-19

Towards New Frontiers in the Exploration of Charmless Non-Leptonic B Decays

Robert Fleischer, [a,b] **Ruben Jaarsma,** [a] **and K. Keri Vos** [a,c,d]

[a] *Nikhef, Science Park 105, NL-1098 XG Amsterdam, Netherlands*
[b] *Department of Physics and Astronomy, Vrije Universiteit Amsterdam, NL-1081 HV Amsterdam, Netherlands*
[c] *Van Swinderen Institute for Particle Physics and Gravity, University of Groningen, NL-9747 AG Groningen, Netherlands*
[d] *Theoretische Physik 1, Naturwissenschaftlich-Technische Fakultät, Universität Siegen, D-57068 Siegen, Germany*

arXiv:1612.07342v1 [hep-ph] 21 Dec 2016

Abstract

Non-leptonic B decays into charmless final states offer an important laboratory to study CP violation and the dynamics of strong interactions. Particularly interesting are $B_s^0 \to K^-K^+$ and $B_d^0 \to \pi^-\pi^+$ decays, which are related by the U-spin symmetry of strong interactions, and allow for the extraction of CP-violating phases and tests of the Standard Model. The theoretical precision is limited by U-spin-breaking corrections and innovative methods are needed in view of the impressive future experimental precision expected in the era of Belle II and the LHCb upgrade. We have recently proposed a novel method to determine the B_s^0–$\bar{B}_s^0$ mixing phase ϕ_s from the $B_s^0 \to K^-K^+$, $B_d^0 \to \pi^-\pi^+$ system, where semileptonic $B_s^0 \to K^-\ell^+\nu_\ell$, $B_d^0 \to \pi^-\ell^+\nu_\ell$ decays are a new ingredient and the theoretical situation is very favourable. We discuss this strategy in detail, with a focus on penguin contributions as well as exchange and penguin-annihilation topologies which can be probed by a variety of non-leptonic B decays into charmless final states. We show that a theoretical precision as high as $\mathcal{O}(0.5^\circ)$ for ϕ_s can be attained in the future, thereby offering unprecedented prospects for the search for new sources of CP violation.

December 2016

Contents

1 Introduction **1**

2 Decay Amplitudes and CP Asymmetries **2**
2.1 Topologies 2
2.2 CP Asymmetries 3
2.3 Untagged Decay Rates 4

3 The Original Strategy **6**
3.1 The UT Angle γ 6
3.2 The B_s^0–$\overline{B}_s^0$ Mixing Phase ϕ_s 8

4 The New Strategy **9**
4.1 Semileptonic Decay Rates 10
4.2 Determination of $\Delta\phi_{KK}$ 12
4.3 Picture from Current Data 15
4.4 News from LHCb 16

5 Insights into Penguin Dynamics **18**
5.1 $B_d^0 \to K^0\overline{K}^0$ and $B_s^0 \to K^0\overline{K}^0$ 18
5.2 $B^+ \to K^+\overline{K}^0$ and $B^+ \to \pi^+K^0$ 21
5.3 $B_d^0 \to \pi^-K^+$ and $B_s^0 \to K^-\pi^+$ 23

6 Insights into Exchange and Penguin Annihilation Dynamics **25**
6.1 Direct Determination from $B_d^0 \to K^-K^+$ and $B_s^0 \to \pi^-\pi^+$ 26
6.2 Indirect Determinations of x 28
6.3 Indirect Information on r'_{PA} 31
6.4 Determination of Ξ_x 34
6.5 Determination of Ξ_P 38

7 Prospects of the New Strategy **39**

8 Conclusions **42**

1 Introduction

CP-violating asymmetries of B mesons are powerful probes in the search for physics beyond the Standard Model (SM) of particle physics. New sources of CP violation might be revealed when comparing the experimental observables determined from different decays with the corresponding SM expectations. Since CP asymmetries are generated through interference effects, non-leptonic decays govern this territory of the B physics landscape. As new heavy particles may well enter the loop contributions (see, for instance, Ref. [1]), decays with penguin topologies are particularly interesting. In order to fully exploit the physics potential of these channels in the era of Belle II [2] and the LHCb upgrade [3], an unprecedented precision of the corresponding SM predictions is essential to match experiment.

The decay $B_s^0 \to K^-K^+$ is dominated by QCD penguin topologies and is hence a particularly promising probe to search for footprints of New Physics (NP) through studies of CP violation. However, the corresponding hadronic parameters suffer from significant theoretical uncertainties through non-perturbative effects. Fortunately, this decay is related to $B_d^0 \to \pi^-\pi^+$ through the U-spin flavour symmetry of the strong interaction, which relates – in analogy to the well-known isospin symmetry – the d and s quarks to each other. Applying the U-spin symmetry, the hadronic parameters characterizing the $B_d^0 \to \pi^-\pi^+$ and $B_s^0 \to K^-K^+$ modes can be related to each other, allowing the extraction of the angle γ of the unitarity triangle (UT) of the Cabibbo–Kobayashi–Maskawa (CKM) matrix and the B_s^0–$\bar{B}_s^0$ mixing phase ϕ_s [4–6]. First measurements of this U-spin method have been performed by the LHCb Collaboration, yielding results for γ and ϕ_s in agreement with the SM and uncertainties at the 7° level [7, 8].

The theoretical precision of this strategy, which is limited by non-factorizable U-spin-breaking corrections, is unfortunately not sufficient to fully exploit the future measurements of CP violation in the $B_d^0 \to \pi^-\pi^+$, $B_s^0 \to K^-K^+$ system at Belle II and the LHCb upgrade. In view of this situation, we have proposed a new method which is very robust with respect to theoretical uncertainties. It uses γ, which can eventually be determined with $\mathcal{O}(1^\circ)$ precision through pure tree decays, as input and allows the determination of ϕ_s with a theoretical precision of up to 0.5° at Belle II and the LHCb upgrade [9]. As the main new ingredient, it uses the $B_d^0 \to \pi^-\pi^+$, $B_s^0 \to K^-K^+$ system in combination with the semileptonic $B_d^0 \to \pi^-\ell^+\nu_\ell$, $B_s^0 \to K^-\ell^+\nu_\ell$ decays. Following these lines, the application of the U-spin symmetry can be limited to theoretically well behaved quantities and valuable tests of the U-spin symmetry can be obtained. As we pointed out in Ref. [9], the current experimental picture is very promising.

In the present paper, we explore the technical details of this new strategy and the attainable precision of ϕ_s in a more comprehensive way. The leading U-spin-breaking corrections enter through a ratio of colour-allowed tree amplitudes, which are well-behaved with respect to factorization and can be analysed within QCD factorization. The major limiting uncertainties enter through certain penguin topologies as well as exchange and penguin-annihilation topologies. The latter are expected to play a minor role in the $B_d^0 \to \pi^-\pi^+$ and $B_s^0 \to K^-K^+$ system on the basis of dynamical arguments [10–12]. Here we present a detailed analysis to constrain these contributions through experimental data, where $B_s^0 \to \pi^-\pi^+$, $B_d^0 \to K^-K^+$ modes play the key role as they emerge exclusively from exchange and penguin-annihilation topologies. In order to determine the relevant penguin contributions, the $B_{s,d}^0 \to K^0\bar{K}^0$ system will be in the spotlight. We will give a roadmap for exploiting the physics information offered by these U-spin-

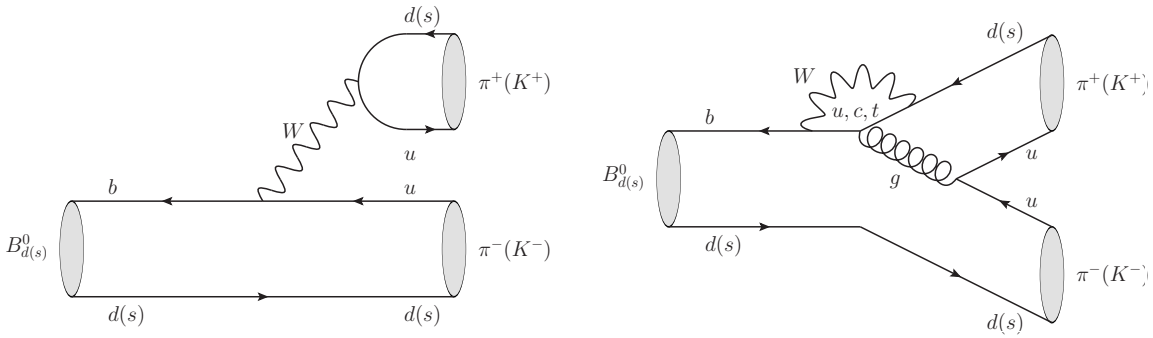

(a) Tree (T)

(b) Penguin (P)

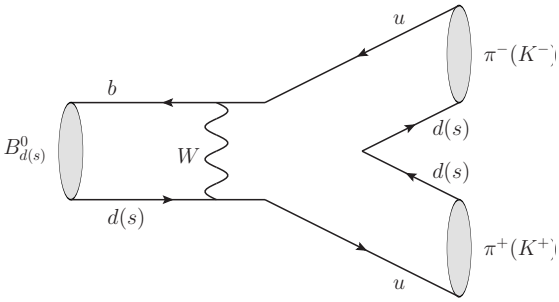

(c) Exchange (E)

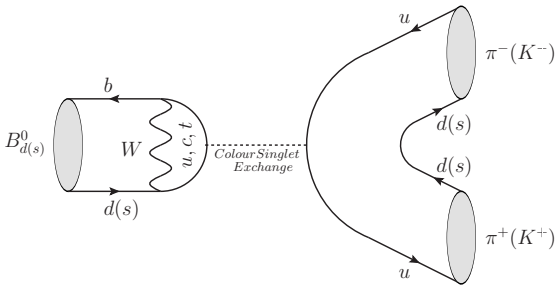

(d) Penguin-annihilation (PA)

Figure 1: Topologies of the $B_d^0 \to \pi^-\pi^+$ and $B_s^0 \to K^-K^+$ decays.

related systems at Belle II and the LHCb upgrade, allowing valuable new insights into hadron dynamics and U-spin-breaking effects.

The outline of this paper is as follows: in Section 2, we introduce the $B_d^0 \to \pi^-\pi^+$ and $B_s^0 \to K^-K^+$ decays and the relevant observables. In Section 3, we discuss the original U-spin strategy and its prospects for the LHCb upgrade. The new strategy is presented in Section 4, exploring also the picture arising from the current data. In Sections 5 and 6, we explore the dynamics of penguin topologies and exchange, penguin-annihilation topologies, respectively. In the latter section, we discuss also the expected pattern of the CP asymmetries in the $B_d^0 \to K^-K^+$, $B_s^0 \to \pi^-\pi^+$ decays and various future scenarios. The prospects of our new strategy are discussed in Section 7, and our main conclusions are summarized in Section 8. Throughout this paper we shall assume that all decay amplitudes are described by their SM expressions.

2 Decay Amplitudes and CP Asymmetries

2.1 Topologies

The non-leptonic decay $B_d^0 \to \pi^-\pi^+$, characterized by a $\bar{b} \to \bar{u}u\bar{d}$ transition, is governed by the decay topologies depicted in Fig. 1. The decay amplitude is dominated by contributions from the tree (T) and penguin (P) topologies, but also receives contributions from exchange (E) and penguin-annihilation (PA) topologies. In the SM, we have [4]

$$A\left(B_d^0 \to \pi^-\pi^+\right) = e^{i\gamma}\mathcal{C}\left[1 - de^{i\theta}e^{-i\gamma}\right] \tag{1}$$

and

$$\mathcal{C} \equiv \lambda^3 A R_b \left[T + E + P^{(ut)} + PA^{(ut)}\right] \tag{2}$$

$$de^{i\theta} \equiv \frac{1}{R_b}\left[\frac{P^{(ct)} + PA^{(ct)}}{T + E + P^{(ut)} + PA^{(ut)}}\right] \tag{3}$$

with

$$P^{(qt)} \equiv P^{(q)} - P^{(t)}, \qquad PA^{(qt)} \equiv PA^{(q)} - PA^{(t)} \ . \tag{4}$$

Both $\mathcal{C}$ and $de^{i\theta}$ are CP-conserving hadronic parameters, while γ provides a CP-violating phase. On the other hand,

$$R_b \equiv \left(1 - \frac{\lambda^2}{2}\right)\frac{1}{\lambda}\left|\frac{V_{ub}}{V_{cb}}\right| = 0.390 \pm 0.030 \tag{5}$$

measures one side of the UT, with λ and A denoting the Wolfenstein parameters of the CKM matrix [13, 14]. For the numerical value, we have used the following results [15]:

$$\lambda \equiv |V_{us}| = 0.22543 \pm 0.00042, \quad A \equiv |V_{cb}|/\lambda^2 = 0.8227^{+0.0066}_{-0.0136}. \tag{6}$$

The decay $B_s^0 \to K^-K^+$ originates from a $\bar{b} \to \bar{u}u\bar{s}$ transition and is related to the $B_d^0 \to \pi^-\pi^+$ channel through the U-spin symmetry [4–6]. In the SM, the $B_s^0 \to K^-K^+$ transition amplitude can be written in the following form:

$$A\left(B_s^0 \to K^-K^+\right) = \sqrt{\epsilon} e^{i\gamma}\mathcal{C}'\left[1 + \frac{1}{\epsilon} d' e^{i\theta'} e^{-i\gamma}\right] , \tag{7}$$

where $\mathcal{C}'$ and $d'e^{i\theta'}$ are the primed equivalents of Eqs. (2) and (3), respectively. The decay topologies are given in Fig. 1. The suppression of the overall amplitude and the enhancement of the penguin parameters $d'e^{i\theta'}$ is given by

$$\epsilon \equiv \frac{\lambda^2}{1-\lambda^2} = 0.0535 \pm 0.0002 \, . \tag{8}$$

The U-spin symmetry [4] implies

$$de^{i\theta} = d'e^{i\theta'} \ , \tag{9}$$

which is only sensitive to non-factorizable U-spin-breaking corrections because the factorizable contributions cancel in these ratios of amplitudes. Contrary, the U-spin relation

$$\mathcal{C} = \mathcal{C}' \tag{10}$$

is affected by both factorizable and non-factorizable U-spin-breaking effects.

2.2 CP Asymmetries

Thanks to quantum-mechanical oscillations between B_q^0 and $\overline{B}_q^0$ mesons, an initially present B_q^0 meson evolves in time into a linear combination of B_q^0 and $\overline{B}_q^0$ states. CP violation is probed by the following time-dependent decay rate asymmetry [16]:

$$\begin{aligned}\mathcal{A}_{\rm CP}(t) &= \frac{|A(B_q^0(t) \to f)|^2 - |A(\bar{B}_q^0(t) \to f)|^2}{|A(B_q^0(t) \to f)|^2 + |A(\bar{B}_q^0(t) \to f)|^2} \\ &= \frac{\mathcal{A}_{\rm CP}^{\rm dir}(B_q \to f)\cos(\Delta M_q t) + \mathcal{A}_{\rm CP}^{\rm mix}(B_q \to f)\sin(\Delta M_q t)}{\cosh(\Delta\Gamma_q t/2) + \mathcal{A}_{\Delta\Gamma}(B_q \to f)\sinh(\Delta\Gamma_q t/2)} \ ,\end{aligned} \tag{11}$$

where $\Delta M_q \equiv M_{\rm H}^{(q)} - M_{\rm L}^{(q)}$ and $\Delta\Gamma_q \equiv \Gamma_{\rm L}^{(q)} - \Gamma_{\rm H}^{(q)}$ denote the mass and decay width differences between the "heavy" and "light" B_q mass eigenstates, respectively.

For the $B_s^0 \to K^-K^+$ channel, we obtain the following expressions [4]:

$$\mathcal{A}_{\rm CP}^{\rm dir}(B_s \to K^-K^+) = \frac{2\epsilon d' \sin\theta' \sin\gamma}{d'^2 + 2\epsilon d' \cos\theta' \cos\gamma + \epsilon^2} \,, \tag{12}$$

$$\mathcal{A}_{\rm CP}^{\rm mix}(B_s \to K^-K^+) = \left[\frac{d'^2 \sin\phi_s + 2\epsilon d' \cos\theta' \sin(\phi_s+\gamma) + \epsilon^2 \sin(\phi_s+2\gamma)}{d'^2 + 2\epsilon d' \cos\theta' \cos\gamma + \epsilon^2}\right] , \tag{13}$$

$$\mathcal{A}_{\Delta\Gamma}(B_s \to K^-K^+) = -\left[\frac{d'^2 \cos\phi_s + 2\epsilon d' \cos\theta' \cos(\phi_s+\gamma) + \epsilon^2 \cos(\phi_s+2\gamma)}{d'^2 + 2\epsilon d' \cos\theta' \cos\gamma + \epsilon^2}\right] . \tag{14}$$

These observables are not independent from one another, satisfying the general relation

$$\left[\mathcal{A}_{\rm CP}^{\rm dir}(B_s \to K^-K^+)\right]^2 + \left[\mathcal{A}_{\rm CP}^{\rm mix}(B_s \to K^-K^+)\right]^2 + \left[\mathcal{A}_{\Delta\Gamma}(B_s \to K^-K^+)\right]^2 = 1 \,. \tag{15}$$

The CP-violating asymmetries for the $B_d^0 \to \pi^-\pi^+$ channel can be straightforwardly obtained through the following replacements:

$$d' \to d \,, \qquad \theta' \to \theta \,, \qquad \phi_s \to \phi_d \,, \qquad \epsilon \to -1 \,. \tag{16}$$

While the direct CP asymmetries $\mathcal{A}_{\rm CP}^{\rm dir}$ of $B_d^0 \to \pi^-\pi^+$ and $B_s^0 \to K^-K^+$ originate from interference between tree and penguin topologies, the mixing-induced CP asymmetries $\mathcal{A}_{\rm CP}^{\rm mix}$ are induced by interference between B_q^0–$\bar{B}_q^0$ mixing and decay processes. The latter observables involve the B_q^0–$\bar{B}_q^0$ mixing phases

$$\phi_d = 2\beta + \phi_d^{\rm NP} \,, \qquad \phi_s = -2\beta_s + \phi_s^{\rm NP} \,, \tag{17}$$

where β is the usual angle of the UT and ϕ_s is a doubly Cabibbo-suppressed phase in the SM. The fits of the UT allow us to calculate the SM value of ϕ_s with high precision [15,17]:

$$\phi_s^{\rm SM} = -2\beta_s = -(2.092^{+0.075}_{-0.069})^\circ \,. \tag{18}$$

The phases $\phi_d^{\rm NP}$ and $\phi_s^{\rm NP}$ describe possible CP-violating NP contributions to B_d^0–$\bar{B}_d^0$ and B_s^0–$\bar{B}_s^0$ mixing, respectively.

2.3 Untagged Decay Rates

Branching ratios contain information from the untagged decay rates [18]. In experiments, the branching ratio is typically defined by using the time-integrated untagged rate, while theoretical expressions require the untagged decay rate at time $t = 0$ [19]. For the B_s meson system there is – in contrast to the B_d-meson system – a sizeable difference between the decay widths of the mass eigenstates [20]:

$$y_s \equiv \frac{\Delta\Gamma_s}{2\Gamma_s} \equiv \frac{\Gamma_{\rm L}^{(s)} - \Gamma_{\rm H}^{(s)}}{2\Gamma_s} = 0.0625 \pm 0.0045. \tag{19}$$

Consequently, the experimental branching ratio needs to be converted into the theoretical branching ratio by means of the following expression [19]:

$$\mathcal{B}(B_s \to f)_{\rm theo} = \left[\frac{1 - y_s^2}{1 + \mathcal{A}_{\Delta\Gamma}^f y_s}\right] \mathcal{B}(B_s \to f)_{\rm exp}. \tag{20}$$

For decays into a flavour-specific final state, such as $B_s^0 \to K^-\pi^+$, only the $[1-y_s^2]$ factor contributes in (20). Using the effective lifetime

$$\tau_f \equiv \frac{\int_0^\infty t\,\langle\Gamma(B_s(t)\to f)\rangle\,dt}{\int_0^\infty \langle\Gamma(B_s(t)\to f)\rangle\,dt} \tag{21}$$

of the B_s decay at hand, the conversion between the experimental and theoretical branching ratios can be obtained with the help of the relation

$$\mathcal{B}(B_s\to f)_{\rm theo} = \left[2-(1-y_s^2)\frac{\tau_f}{\tau_{B_s}}\right]\mathcal{B}(B_s\to f)_{\rm exp}, \tag{22}$$

which does not explicitly depend on the $\mathcal{A}^f_{\Delta\Gamma}$ observable [19].

For the conversion of the experimental $B_s^0\to K^-K^+$ branching ratio into its theoretical counterpart, we use the measurement of the LHCb Collaboration [21]

$$\tau_{K^+K^-} = [1.407\pm 0.016\ ({\rm stat})\ \pm 0.007\ ({\rm syst})]\,{\rm ps}, \tag{23}$$

which leads to a difference between the experimental and theoretical branching ratios of about 7%.

It is useful to introduce the following quantity [5, 6]:

$$\begin{aligned} K &\equiv \frac{1}{\epsilon}\left|\frac{\mathcal{C}}{\mathcal{C}'}\right|^2\left[\frac{m_{B_s}}{m_{B_d}}\frac{\Phi(m_\pi/m_{B_d},m_\pi/m_{B_d})}{\Phi(m_K/m_{B_s},m_K/m_{B_s})}\frac{\tau_{B_d}}{\tau_{B_s}}\right]\frac{\mathcal{B}(B_s\to K^-K^+)_{\rm theo}}{\mathcal{B}(B_d\to\pi^-\pi^+)}\\ &= \frac{1+2(d'/\epsilon)\cos\theta'\cos\gamma+(d'/\epsilon)^2}{1-2d\cos\theta\cos\gamma+d^2}, \end{aligned} \tag{24}$$

where

$$\Phi(X,Y) = \sqrt{[1-(X+Y)^2][1-(X-Y)^2]} \tag{25}$$

is the usual phase-space function. The factorizable U-spin-breaking contributions to the ratio $|\mathcal{C}/\mathcal{C}'|$ are given as follows:

$$\left|\frac{\mathcal{C}}{\mathcal{C}'}\right|_{\rm fact} = \frac{f_\pi}{f_K}\left[\frac{m_{B_d}^2-m_\pi^2}{m_{B_s}^2-m_K^2}\right]\left[\frac{F_0^{B_d\pi}(m_\pi^2)}{F_0^{B_sK}(m_K^2)}\right] = 0.71^{+0.06}_{-0.11}, \tag{26}$$

where we have used the QCD light-cone sum rule (LCSR) calculation $F_0^{B_sK}(0)/F_0^{B_d\pi}(0) = 1.15^{+0.17}_{-0.09}$ [22], which is in agreement with previous results in [23], and $f_K/f_\pi = 1.1928\pm 0.0026$ [24]. The form factors for the $\bar B_d^0\to\pi^+$ transition are defined through

$$\begin{aligned} \left\langle\pi^+(k)|\bar u\gamma_\mu b|\bar B_d^0(p)\right\rangle &= F_0^{B_d\pi}(q^2)\left(\frac{m_{B_d}^2-m_\pi^2}{q^2}\right)q_\mu\\ &+F_1^{B_d\pi}(q^2)\left[(p+k)_\mu-\left(\frac{m_{B_d}^2-m_\pi^2}{q^2}\right)q_\mu\right] \end{aligned} \tag{27}$$

with $q\equiv p-k$; the $\bar B_s^0\to K^+$ form factors $F_{0,1}^{B_sK}(q^2)$ are defined in an analogous way. Finally, we obtain

$$K \stackrel{\rm exp}{=} 51.4^{+9.0}_{-15.7}\ , \tag{28}$$

	Current [20, 30]	Upgrade [3]
$\mathcal{A}_{\rm CP}^{\rm dir}(B_d \to \pi^-\pi^+)$	-0.31 ± 0.05	-0.31 ± 0.008
$\mathcal{A}_{\rm CP}^{\rm mix}(B_d \to \pi^-\pi^+)$	0.66 ± 0.06	0.66 ± 0.008
$\mathcal{A}_{\rm CP}^{\rm dir}(B_s \to K^-K^+)$	0.14 ± 0.11	0.087 ± 0.008
$\mathcal{A}_{\rm CP}^{\rm mix}(B_s \to K^-K^+)$	-0.30 ± 0.13	-0.19 ± 0.008

Table 1: Overview of the current measurements and the expected accuracy at the LHCb upgrade. The upgrade central values for $B_s^0 \to K^-K^+$ are calculated by applying the U-spin symmetry to (d, θ) obtained from the $B_d^0 \to \pi^-\pi^+$ CP asymmetries.

where we have neglected non-factorizable U-spin-breaking corrections to the ratio $|\mathcal{C}/\mathcal{C}'|$. We shall return to this quantity in Section 7. Using the U-spin relations in Eq. (9), we may also write

$$K = -\frac{1}{\epsilon}\left[\frac{\mathcal{A}_{\rm CP}^{\rm dir}(B_d \to \pi^-\pi^+)}{\mathcal{A}_{\rm CP}^{\rm dir}(B_s \to K^-K^+)}\right] \stackrel{\rm exp}{=} 41.4 \pm 33.2 \ , \tag{29}$$

which is in agreement with Eq. (28), but has a much larger error due to the currently large uncertainties of the $B_s^0 \to K^-K^+$ CP asymmetries.

3 The Original Strategy

Before discussing the new method, it is instructive to have a closer look at the original strategy [4–6], where γ and ϕ_s can be extracted from the $B_d^0 \to \pi^-\pi^+$, $B_s^0 \to K^-K^+$ system with the help of the U-spin symmetry. Using information on the corresponding branching ratios, CP violation in the $B_d^0 \to \pi^-\pi^+$ mode and the first measurement of CP violation in the $B_s^0 \to K^-K^+$ channel [7], the LHCb collaboration has reported the following results [8]:

$$\gamma = (63.5^{+7.2}_{-6.7})^\circ, \qquad \phi_s = -(6.9^{+9.2}_{-8.0})^\circ \ , \tag{30}$$

which are in agreement with the picture of the previous analyses in Refs. [4–6].

3.1 The UT Angle γ

The UT angle γ can be determined in a theoretically clean way from pure tree decays of the kind $B \to D^{(*)}K^{(*)}$ [25, 26] (for an overview, see [27]). The averages of the corresponding experimental results performed by the CKMfitter [28] and UTfit [29] collaborations yield

$$\gamma = (73.2^{+6.3}_{-7.0})^\circ \qquad \text{and} \qquad \gamma = (68.3 \pm 7.5)^\circ, \tag{31}$$

respectively. The results in (31) are in remarkable agreement with the γ measurement in (30), and it is interesting to note that the current uncertainties of both determinations are at the same level. In the future era of Belle II and the LHCb upgrade, the uncertainty of the γ determination from pure $B \to D^{(*)}K^{(*)}$ tree decays can be reduced to the 1° level, which is very impressive [2, 3].

The current values of the CP asymmetries [20, 30] are listed in Table 1. Let us now explore the prospects of the U-spin strategy. Contrary to the pure tree determination of γ, the $B_d^0 \to \pi^-\pi^+$, $B_s^0 \to K^-K^+$ system obtains significant contributions from penguin loop topologies, which may receive NP contributions. Within the current precision at

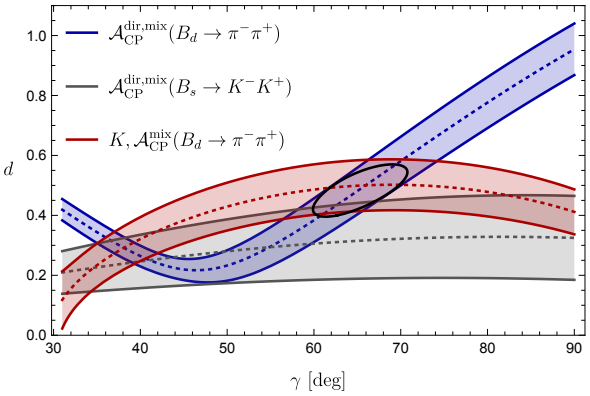

Figure 2: Illustration of the determination of γ from the CP asymmetries of $B_d^0 \to \pi^-\pi^+$, $B_s^0 \to K^-K^+$ and the observable K for the current data.

the level of 7°, there is not any sign of CP-violating NP effects of this kind in the data and an effort has to be made to achieve a much higher precision.

Let us use the mixing phases $\phi_d = 43.2 \pm 1.8$ [31], as determined from $B_{d,s}^0 \to J/\psi K_s^0$ decays by taking penguin effects into account, and the PDG average $\phi_s = -(0.68 \pm 2.2)°$ [30] (see Subsection 3.2). Moreover, we assume the U-spin relations in Eq. (9). In Fig. 2, we show the contours in the d–γ plane which can then be fixed – in a theoretically clean way – through the CP asymmetries of the $B_d^0 \to \pi^-\pi^+$ and $B_s^0 \to K^-K^+$ decays. We observe that currently only poor constraints on γ can be obtained by using only the CP asymmetries, which is mainly due to the large uncertainty of the CP violation measurements of the $B_s^0 \to K^-K^+$ channel.

Consequently, the current LHCb determination in Eq. (30) is governed by CP violation in $B_d^0 \to \pi^-\pi^+$ and the branching ratio information encoded in the K observable given in Eq. (24). We illustrate this feature in Fig. 2, where we have used the value of K in Eq. (28)[1], containing the factorizable form-factor contributions to the ratio $|\mathcal{C}/\mathcal{C}'|$ given in Eq. (26). We have neglected any non-factorizable contributions to $|\mathcal{C}/\mathcal{C}'|$, and have assumed the U-spin relations in Eq. (9). In Fig. 2, we show also the 1σ contour from a χ^2 fit to the current data. We obtain the following results:

$$\gamma = (66^{+5}_{-6})°, \qquad d = 0.49^{+0.08}_{-0.09}, \qquad \theta = (147^{+7}_{-10})° \ , \tag{32}$$

where γ is in agreement with Eq. (30).

As we can see from the fit, the determination of γ in Eq. (32) is essentially fully driven by the CP asymmetries of $B_d^0 \to \pi^-\pi^+$ and K, while CP violation in $B_s^0 \to K^-K^+$ has a minor impact. To quantify this, we perform a χ^2 fit to only the CP asymmetries of $B_d^0 \to \pi^-\pi^+$ and K. We then find

$$\gamma = (66^{+5}_{-6})°, \qquad d = 0.50^{+0.09}_{-0.10}, \qquad \theta = (147^{+8}_{-10})° \ , \tag{33}$$

which is in very good agreement with the results in Eq. (32). This now allows us to determine the CP asymmetries of $B_s^0 \to K^-K^+$. Employing the U-spin relations in Eq. (9) yields

$$\begin{aligned}
\mathcal{A}_{\rm CP}^{\rm dir}(B_s \to K^-K^+) &= 0.11^{+0.03}_{-0.02}|_d \, {}^{+0.03}_{-0.02}|_\theta \, {}^{+0.00}_{-0.00}|_\gamma = 0.11^{+0.04}_{-0.03} \\
\mathcal{A}_{\rm CP}^{\rm mix}(B_s \to K^-K^+) &= -0.18^{+0.03}_{-0.04}|_d \, {}^{+0.02}_{-0.02}|_\theta \, {}^{+0.01}_{-0.01}|_\gamma = -0.18^{+0.04}_{-0.04} \ .
\end{aligned} \tag{34}$$

[1]To be conservative, we consider only the largest uncertainty for K in Eq. (28).

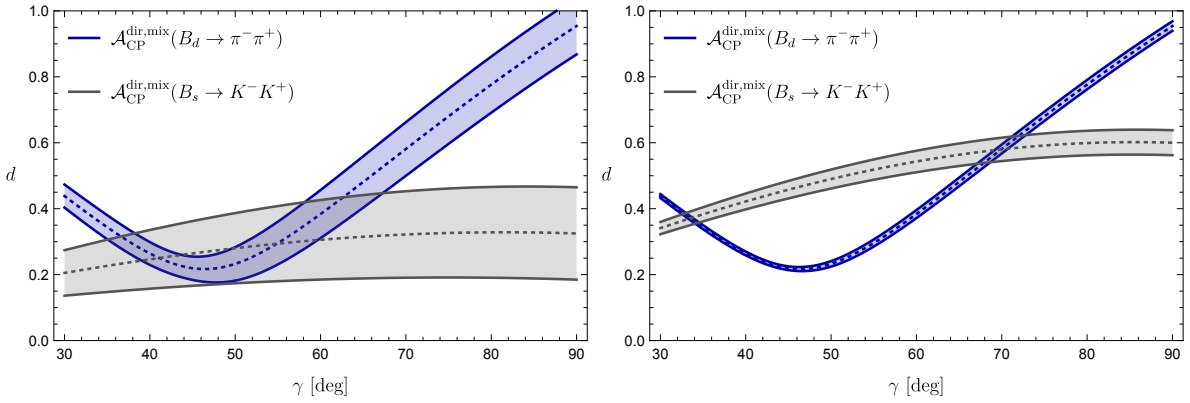

(a) Current situation (b) Upgrade situation

Figure 3: Illustration of the determination of γ from the CP asymmetries of $B_d^0 \to \pi^-\pi^+$ and $B_s^0 \to K^-K^+$ as given in Table 1.

In view of the expected much more precise measurements of the CP asymmetries of $B_s^0 \to K^-K^+$ at the LHCb upgrade there is great potential in this strategy. In fact, the K observable can then be avoided and γ can be extracted using only the CP asymmetries of $B_d^0 \to \pi^-\pi^+$ and $B_s^0 \to K^-K^+$, thereby resulting in a much more favourable situation [4–6]. In Fig. 3, we compare the contours from the $B_d^0 \to \pi^-\pi^+$ and $B_s^0 \to K^-K^+$ CP asymmetries for (a) the current situation, and (b) the LHCb upgrade scenario with $\phi_s = -(2.1 \pm 0.5)^\circ$, as given in Table 1. In this scenario, we use the expected uncertainties given in [3], and we use the U-spin relations in Eq. (9) combined with Eqs. (12) and (13) to calculate the central values for the $B_s^0 \to K^-K^+$ CP asymmetries, because of the large current uncertainties. Assuming the U-spin relation $d = d'$, the upgrade scenario leads to $\gamma = (69.9^{+2.4}_{-2.1})^\circ$ [2]. However, U-spin-breaking corrections limit the precision of γ. In order to illustrate these effects, we parametrize them as

$$\xi \equiv \frac{d'}{d}, \qquad \Delta \equiv \theta' - \theta, \tag{35}$$

and consider U-spin breaking effects of 20%, i.e. $\xi = 1.0 \pm 0.2$ and $\Delta = (0 \pm 20)^\circ$. This leads to $\gamma = (70^{+8}_{-6})^\circ$, which is comparable to the current situation described above.

The impact of U-spin-breaking contributions was also studied in Ref. [32], where the U-spin method was combined with the $B \to \pi\pi$ isospin analysis [33] to reduce U-spin breaking effects. In Ref. [8], it was found that the corresponding results agree with Ref. [4] for corrections of up to 50%, while the $B \to \pi\pi$ system stabilizes the situation for even larger corrections. We shall discuss U-spin-breaking effects in more detail below, showing that such anomalously large effects are not supported by the experimental data.

3.2 The B_s^0–$\overline{B}_s^0$ Mixing Phase ϕ_s

The phase ϕ_s can be determined from $B_s^0 \to J/\psi\phi$ and decays with similar dynamics, which are dominated by tree topologies [34, 35]. The theoretical precision is limited by penguin contributions (see Ref. [31] and references therein). The current average from the Particle Data Group (PDG) [30] reads

$$\phi_s = -(0.68 \pm 2.2)^\circ, \tag{36}$$

[2] A somewhat better precision is reached if the value of γ is lower.

which is in agreement with the LHCb result in Eq. (30). In the future, we may extract ϕ_s from CP-violating effects in $B_s^0 \to J/\psi\phi$ and penguin control channels with a precision as high as $\mathcal{O}(0.5^\circ)$ [31].

The B_s^0–$\bar{B}_s^0$ mixing phase can also be extracted from $B_s^0 \to K^-K^+$ decays. The corresponding CP asymmetries allow us to determine the "effective mixing phase"

$$\phi_s^{\rm eff} \equiv \phi_s + \Delta\phi_{KK} \tag{37}$$

through

$$\sin\phi_s^{\rm eff} = \frac{\mathcal{A}_{\rm CP}^{\rm mix}(B_s \to K^-K^+)}{\sqrt{1-\mathcal{A}_{\rm CP}^{\rm dir}(B_s \to K^-K^+)^2}}\,, \tag{38}$$

where the hadronic phase shift $\Delta\phi_{KK}$ takes the following form [31, 36, 37]:

$$\tan\Delta\phi_{KK} = 2\epsilon\sin\gamma\left[\frac{d'\cos\theta' + \epsilon\cos\gamma}{d'^2 + 2\epsilon d'\cos\theta'\cos\gamma + \epsilon^2\cos 2\gamma}\right]\,. \tag{39}$$

Let us now use $\gamma = (70\pm1)^\circ$ and $\phi_d = (43.2\pm0.6)^\circ$ [31] as an input. Using also Table 1, we then find for the LHCb upgrade scenario

$$\phi_s^{\rm eff} = -(11.0\pm0.5)^\circ\,, \tag{40}$$

which would match the expected precision for ϕ_s from $B_s^0 \to J/\psi\phi$ and related decays. However, in order to extract ϕ_s from this phase, we need the hadronic phase shift $\Delta\phi_{KK}$. It can be calculated by applying the U-spin symmetry to d and θ extracted from the $B_d^0 \to \pi^-\pi^+$ CP asymmetries. Assuming U-spin-breaking corrections of 20% as before, i.e. $\xi = 1.0\pm0.2$ and $\Delta = 0\pm20^\circ$, yields

$$\Delta\phi_{KK} = -(8.9\pm2.6)^\circ\,, \tag{41}$$

leading to $\phi_s = -(2.1\pm2.6)^\circ$. Consequently, we cannot match the precision of ϕ_s from $B_s^0 \to J/\psi\phi$ and related decays due to the U-spin-breaking corrections and cannot fully exploit the experimental precision at the LHCb upgrade. To this end, an innovative method is needed, which we describe in the next section.

4 The New Strategy

In order to take full advantage of the huge amount of data to be collected at Belle II and the LHCb upgrade, we proposed a new strategy for the $B_d^0 \to \pi^-\pi^+$, $B_s^0 \to K^-K^+$ system. It uses γ as an input and makes minimal use of the U-spin symmetry, allowing the extraction of the B_s^0–$\bar{B}_s^0$ mixing phase ϕ_s with a future theoretical precision as high as $\mathcal{O}(0.5^\circ)$ [9]. Moreover, valuable insights into U-spin-breaking effects can be obtained. The new key elements are the differential rates of the semileptonic decays $B_s^0 \to K^-\ell^+\nu_\ell$ and $B_d^0 \to \pi^-\ell^+\nu_\ell$, which we combine with the $B_s^0 \to K^-K^+$ and $B_d^0 \to \pi^-\pi^+$ decay rates; the corresponding information is encoded in observables R_K and R_π, respectively. The flow chart of this strategy is shown in Fig. 4.

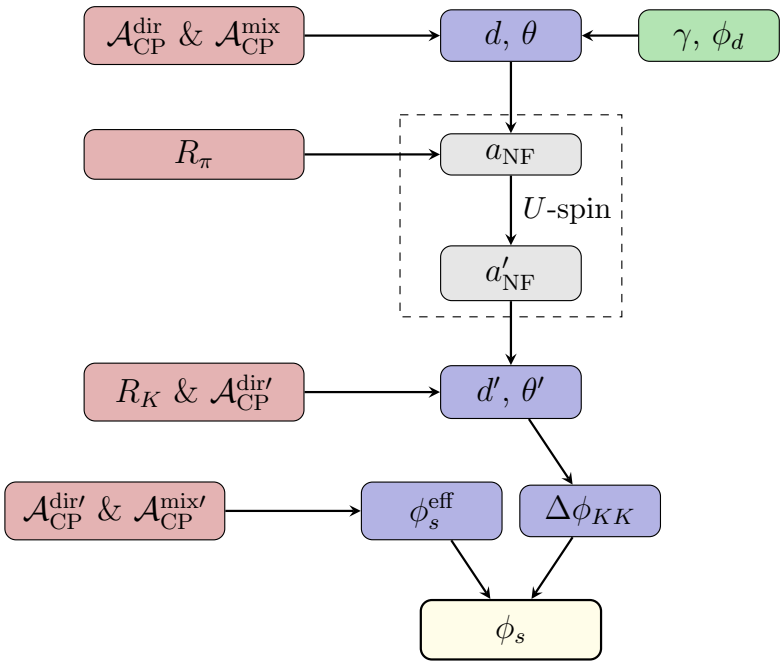

Figure 4: Flowchart of the new strategy as discussed in detail in Section 4. The $\mathcal{A}_{\rm CP}^{\rm dir}$, $\mathcal{A}_{\rm CP}^{\rm mix}$ and $\mathcal{A}_{\rm CP}^{\rm dir\,\prime}$, $\mathcal{A}_{\rm CP}^{\rm mix\prime}$ denote the direct, mixing-induced CP asymmetries of the decays $B_d^0 \to \pi^-\pi^+$ and $B_s^0 \to K^-K^+$, respectively.

4.1 Semileptonic Decay Rates

For the upgrade scenario, we assume a determination of $\gamma = (70 \pm 1)^\circ$ from the pure tree decays [3]. In addition, we use $\phi_d = (43.2 \pm 0.6)^\circ$ [31], as well as the CP asymmetries given for the upgrade in Table 1. These inputs allow a determination of d and θ from the $B_d^0 \to \pi^-\pi^+$ CP asymmetries [4]. We find

$$d = 0.58 \pm 0.02, \qquad \theta = (151.4 \pm 1.1)^\circ\,, \tag{42}$$

where the precision for these non-perturbative parameters is remarkable.

Additional information is encoded in the branching ratios, as we have seen in Eq. (24). However, the observable K is affected by the U-spin-breaking form-factor ratio, as well as non-factorizable effects. It is more advantageous to consider ratios of non-leptonic decay rates with respect to differential rates of semileptonic modes, as was done for an extensive analysis of $B \to D\bar{D}$ decays in Ref. [37]. These ratios also provide a well-known test for the factorisation of hadronic matrix elements of non-leptonic decays [38–45].

For our transitions at hand, we define

$$R_\pi \equiv \frac{\Gamma(B_d \to \pi^-\pi^+)}{|d\Gamma(B_d^0 \to \pi^-\ell^+\nu_\ell)/dq^2|_{q^2=m_\pi^2}} = 6\pi^2 |V_{ud}|^2 f_\pi^2 X_\pi r_\pi |a_{\rm NF}|^2\,, \tag{43}$$

where

$$r_\pi \equiv 1 + d^2 - 2d\cos\theta\cos\gamma\,, \tag{44}$$

f_π denotes the charged pion decay constant, V_{ud} is the corresponding CKM matrix element, and

$$X_\pi \equiv \frac{(m_{B_d}^2 - m_\pi^2)^2}{m_{B_d}^2(m_{B_d}^2 - 4m_\pi^2)} \left[\frac{F_0^{B_d\pi}(m_\pi^2)}{F_1^{B_d\pi}(m_\pi^2)}\right]^2\,. \tag{45}$$

Decay	Branching ratio
$B_d \to \pi^-\pi^+$	$(5.12 \pm 0.19) \times 10^{-6}$
$B_d \to \pi^- K^+$	$(1.96 \pm 0.05) \times 10^{-5}$
$B_d \to K^- K^+$	$(8.03 \pm 1.49) \times 10^{-8}$
$B_s \to K^- K^+$	$(2.49 \pm 0.17) \times 10^{-5}$
$B_s \to K^- \pi^+$	$(5.5 \pm 0.6) \times 10^{-6}$
$B_s \to \pi^- \pi^+$	$(6.71 \pm 0.83) \times 10^{-7}$
$B^\pm \to K^\pm K$	$(1.32 \pm 0.14) \times 10^{-6}$
$B^\pm \to \pi^\pm K$	$(23.79 \pm 0.75) \times 10^{-6}$

Table 2: Overview of the experimental branching ratios [20, 30]. For the $B_d^0 \to K^- K^+$ and $B_s^0 \to \pi^-\pi^+$ modes recent LHCb results [49] were used to calculate new averages according to the PDG method [30].

The form factors were defined in Eq. (27), and satisfy the relation

$$\frac{F_0^{B_d\pi}(0)}{F_1^{B_d\pi}(0)} = 1 \tag{46}$$

due to kinematic constraints which are also implemented in lattice QCD calculations [46, 47]. We assume $F_0^{B_d\pi}(m_\pi^2)/F_1^{B_d\pi}(m_\pi^2) = 1$, i.e. a negligible deviation from this result for the small momentum transfer $q^2 = m_\pi^2$. The non-factorizable contributions are parameterized by the following quantity:

$$a_{\rm NF} \equiv (1 + r_P)(1 + x) a_{\rm NF}^T \ , \tag{47}$$

where

$$r_P \equiv \frac{P^{(ut)}}{T} \ , \qquad x \equiv |x| e^{i\sigma} \equiv \frac{E + PA^{(ut)}}{T + P^{(ut)}} \ . \tag{48}$$

The non-factorizable contributions to the colour-allowed tree topology T are characterized by the deviation of $a_{\rm NF}^T$ from one. This parameter can be described within the QCD factorization framework [42, 43]. The current state-of-the-art calculation [44], including two-loop (NNLO) QCD effects, yields

$$a_{\rm NF}^T = 1.000^{+0.029}_{-0.069} + (0.011^{+0.023}_{-0.050}) i \ . \tag{49}$$

The colour-allowed tree amplitude is theoretically very favourable with respect to the factorization of hadronic matrix elements, which is also reflected by the sophisticated analysis devoted to the parameter in (49). On the other hand, penguin topologies are much more challenging and are affected by non-factorizable effects and long-distance contributions, such as those attributed to "charming penguins" [48].

The branching ratio of the $B_d^0 \to \pi^-\pi^+$ channel is given in Table 2. The differential decay rate at low q^2 unfortunately suffers from sizable experimental uncertainties. We may estimate the required partial branching fraction of the semileptonic rate by averaging the low q^2 measurements of the BaBar and Belle collaborations [30, 50, 51]. We find $d{\rm BR}/dq^2 \sim (6 \pm 1){\rm GeV}^{-2}$. A more sophisticated analysis of this quantity lies outside the scope of this paper. However, we note that our estimate is in agreement with the analyses in, e.g., Refs. [52] and [53], where this rate is used to extract the CKM matrix element $|V_{ub}|$. Finally, we obtain

$$R_\pi = (0.85 \pm 0.15){\rm GeV}^2 \ , \tag{50}$$

which corresponds to a relative error of 17%. We advocate to extract this ratio directly from the experimental Belle (II) and LHCb data.

Using (d, θ) from the $B_d^0 \to \pi^-\pi^+$ CP asymmetries in Eq. (42), we may extract r_π in Eq. (44). Combining this parameter with R_π and the experimental value for [24]

$$|V_{ud}| f_\pi = (127.13 \pm 0.02 \pm 0.13)\text{MeV} \tag{51}$$

gives

$$|a_{\rm NF}| = 0.73 \pm 0.06 \ . \tag{52}$$

Concerning $B_s^0 \to K^-K^+$, we introduce in analogy to R_π the following ratio:

$$R_K \equiv \frac{\Gamma(B_s \to K^-K^+)}{|d\Gamma(B_s^0 \to K^-\ell^+\nu_\ell)/dq^2|_{q^2=m_K^2}} = 6\pi^2 |V_{us}|^2 f_K^2 X_K r_K |a'_{\rm NF}|^2 \ , \tag{53}$$

where

$$r_K \equiv 1 + \left(\frac{d'}{\epsilon}\right)^2 + 2\frac{d'}{\epsilon}\cos\theta'\cos\gamma \ , \tag{54}$$

$$X_K \equiv \frac{(m_{B_s}^2 - m_K^2)^2}{m_{B_s}^2(m_{B_s}^2 - 4m_K^2)} \left[\frac{F_0^{B_sK}(m_K^2)}{F_1^{B_sK}(m_K^2)}\right]^2 \ , \tag{55}$$

f_K denotes the charged kaon decay constant, and V_{us} is the corresponding CKM matrix element.

4.2 Determination of $\Delta\phi_{KK}$

In order to determine the hadronic parameters d' and θ' of the $B_s^0 \to K^-K^+$ decay, we use the following expression:

$$r_K = r_\pi \frac{R_K}{R_\pi}\left[\frac{|V_{ud}| f_\pi}{|V_{us}| f_K}\right]^2 \frac{X_\pi}{X_K}(\xi_{\rm NF}^a)^2 \ . \tag{56}$$

As we have seen above, r_π can be determined from the CP asymmetries in $B_d^0 \to \pi^-\pi^+$, and the only unknown quantity in the game is the following parameter [9]:

$$\xi_{\rm NF}^a \equiv \left|\frac{a_{\rm NF}}{a'_{\rm NF}}\right| = \left|\frac{1 + r_P}{1 + r_P'}\right| \left|\frac{1 + x}{1 + x'}\right| \left|\frac{a_{\rm NF}^T}{a_{\rm NF}^{T'}}\right| \ . \tag{57}$$

It can be determined with the help of the U-spin symmetry. We will show below that $\xi_{\rm NF}^a$ has actually a structure which is very favourable with respect to U-spin-breaking corrections. We may then determine r_K, which we may combine with the direct CP asymmetry of the $B_s^0 \to K^-K^+$ decay to extract its hadronic parameters d' and θ':

$$d' = \epsilon\left[r_K + \cos 2\gamma \pm \sqrt{(r_K + \cos 2\gamma)^2 - (r_K - 1)^2 - (r_K \mathcal{A}_{\rm CP}^{\rm dir\prime}/\tan\gamma)^2}\right]^{1/2} \ , \tag{58}$$

$$\cos\theta' = \frac{\epsilon^2(r_K - 1) - d'^2}{2\epsilon d'\cos\gamma}, \qquad \sin\theta' = \frac{\epsilon r_K \mathcal{A}_{\rm CP}^{\rm dir\prime}}{2d'\sin\gamma} \, . \tag{59}$$

Here we have defined $\mathcal{A}_{\rm CP}^{\rm dir\prime} \equiv \mathcal{A}_{\rm CP}^{\rm dir}(B_s \to K^-K^+)$. Finally, we may calculate the hadronic phase shift $\Delta\phi_{KK}$ using Eq. (39), which yields

$$\tan\Delta\phi_{KK} = \frac{2\sin\gamma}{\epsilon}\left[\frac{d'\cos\theta' + \epsilon\cos\gamma}{r_K - 1 + \cos 2\gamma}\right] \ . \tag{60}$$

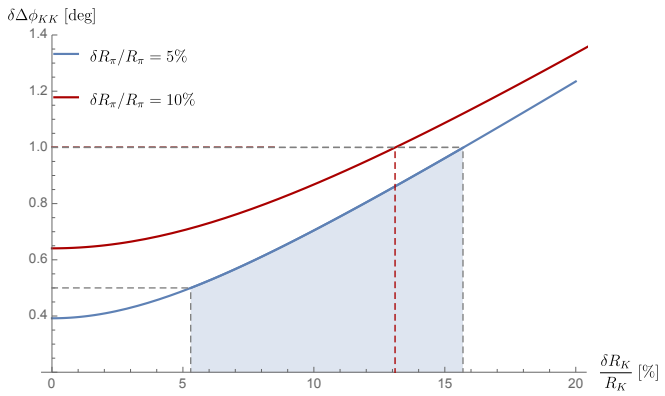

Figure 5: The experimental error for $\Delta\phi_{KK}$ as a function of the relative precision of R_K for a relative precision of R_π of 5% and 10%, assuming a perfect theoretical situation.

The B_s^0–$\bar{B}_s^0$ mixing phase $\phi_s = \phi_s^{\rm eff} - \Delta\phi_{KK}$ can then be extracted from the measured effective mixing phase $\phi_s^{\rm eff}$.

Unfortunately, the semileptonic decay $B_s^0 \to K^-\ell^+\nu_\ell$ has not yet been measured. We advocate analyses of this channel at Belle (II) and LHCb, preferably by a direct measurement of the double ratio R_π/R_K. Here only the double ratio of the form factors enters through X_π/X_K, which strongly reduces the sensitivity to small deviations from (46) for the momentum transfers $q^2 = m_\pi^2$ and m_K^2, thereby yielding a double ratio of form factors equal to one with excellent precision. In addition, the ratio $|V_{us}|f_K/|V_{ud}|f_\pi = 0.27599 \pm 0.00037$ can be determined with tiny uncertainties from experimental data [24]. It is interesting to note that R_K does not depend on the ratio of the $B_{s,d}^0$ fragmentation functions f_s/f_d, which is the major limiting factor for measurements of B_s^0 branching ratios [54].

We illustrate the future experimental precision for $\Delta\phi_{KK}$ that can eventually be achieved with our new strategy for a perfect theoretical situation in Fig. 5. There we show the sensitivity as a function of the relative precision of R_K, while assuming measurements of R_π in the upgrade era with relative precisions of 5% and 10%. Getting to the precision of 0.5° for $\Delta\phi_{KK}$ requires a determination of R_K and R_π with a relative error of 5%. In Fig. 6, we show the experimental error budget of $\Delta\phi_{KK}$, considering a relative error of 5% for R_K and R_π.

Interestingly, for values of γ around 70°, the dependence of $\Delta\phi_{KK}$ on γ is essentially negligible. This can be understood as $\tan\Delta\phi_{KK}$ in Eq. (60) is then given by

$$\tan\Delta\phi_{KK} \sim \frac{2\sin\gamma}{\sqrt{r_K}}, \tag{61}$$

while

$$r_K \propto r_\pi \propto \sin^2\gamma. \tag{62}$$

Consequently, if we used ϕ_s as an input for our strategy and were aiming to determine γ, we would have a small sensitivity for this angle. It is hence much more advantageous to use γ as input and determine ϕ_s.

The theoretical precision of the new strategy is limited by the U-spin-breaking corrections affecting $\xi_{\rm NF}^a$ in Eq. (57). The structure of $\xi_{\rm NF}^a$, which depends on

$$\Xi_P \equiv \left|\frac{1+r_P}{1+r_P'}\right|, \qquad \Xi_x \equiv \left|\frac{1+x}{1+x'}\right|, \tag{63}$$

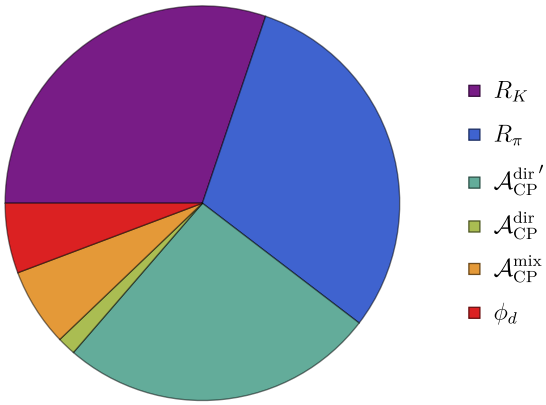

Figure 6: Experimental error budget for $\Delta\phi_{KK}$. Here we have assumed a relative precision of 5% for R_K and R_π and a perfect theoretical situation.

and the ratio of the non-factorizable, colour-allowed tree-level contributions, is very favourable in this respect. As both r_P and x are small parameters, the ratios entering Eq. (57) are very robust concerning U-spin-breaking corrections. We will come back to this feature in Subections 6.4 and 6.5 after we have explored the implications of the current data for r_P and x.

Corrections to the U-spin relation $a_{\rm NF}^{T} = a_{\rm NF}^{T'}$ for the non-factorizable contributions to the colour-allowed tree amplitudes can be quantified within the framework of QCD factorization [44]. So far only the $B_d^0 \to \pi^-\pi^+$ decay has been analyzed, with the result in Eq. (49). Following Ref. [9], we write

$$a_{\rm NF}^{T(\prime)} = 1 + \Delta_{\rm NF}^{T(\prime)} \tag{64}$$

with $\Delta_{\rm NF}^{T'} = \Delta_{\rm NF}^{T}(1 - \xi_{\rm NF}^{T})$, such that we obtain

$$\frac{a_{\rm NF}^{T}}{a_{\rm NF}^{T'}} = 1 + \Delta_{\rm NF}^{T}\xi_{\rm NF}^{T} + \mathcal{O}((\Delta_{\rm NF}^{T})^2)\ . \tag{65}$$

Using Eq. (49), we estimate $\Delta_{\rm NF}^{T} \sim 0.05$. Allowing for U-spin-breaking corrections of 20% for the non-factorizable contributions gives a tiny correction of $\mathcal{O}(1\%)$ to the ratio in Eq. (65). Even larger U-spin-breaking corrections would not have a significant impact on this picture. It would be interesting to extend the QCD factorization analysis of the colour-allowed tree amplitude to the $B_s^0 \to K^-K^+$ decay.

The advantage of our new strategy concerning U-spin-breaking effects in comparison with the original method can be clearly seen by rewriting the parameter ξ in Eq. (35) as

$$\xi = \xi_{\rm NF}^{a} \left|\frac{T_{\rm fact}}{T'_{\rm fact}}\right| \left|\frac{P^{(ct)\prime} + PA^{(ct)\prime}}{P^{(ct)} + PA^{(ct)}}\right|. \tag{66}$$

Here the leading U-spin-breaking corrections are associated with penguin topologies, which are challenging, with issues such as "charming" penguins [48]. Therefore, the uncertainty of $\xi_{\rm NF}^{a}$ is significantly smaller than that of ξ.

4.3 Picture from Current Data

Since the differential semileptonic $B_s^0 \to K^0 \ell^+ \nu_\ell$ decay rate has not yet been measured, we cannot apply our new strategy to current data. However, as a demonstration, we can consider the $B_d^0 \to \pi^- K^+$ decay. This channel only receives contributions from tree and penguin topologies. Neglecting exchange and penguin-annihilation contributions to $B_s^0 \to K^- K^+$, the $B_d^0 \to \pi^- K^+$ decay topologies only differ at the spectator-quark level. The transition amplitude can be written as follows [4, 5]:

$$A(B_d^0 \to \pi^- K^+) = \sqrt{\epsilon} e^{i\gamma} \tilde{\mathcal{C}}' \left[1 + \frac{1}{\epsilon} \tilde{d}' e^{i\tilde{\theta}'} e^{-i\gamma}\right] \tag{67}$$

with

$$\tilde{\mathcal{C}}' \equiv \lambda^3 A R_b \left[\tilde{T}' + \tilde{P}^{(ut)\prime}\right] , \qquad \tilde{d}' e^{i\tilde{\theta}'} \equiv \frac{1}{R_b} \left[\frac{\tilde{P}^{(ct)\prime}}{\tilde{T}' + \tilde{P}^{(ut)\prime}}\right] . \tag{68}$$

Using Eq. (7) and the $SU(3)$ relation

$$\frac{P^{(ct)\prime}}{T' + P^{(ut)\prime}} = \frac{\tilde{P}^{(ct)\prime}}{\tilde{T}' + \tilde{P}^{(ut)\prime}} \tag{69}$$

gives

$$\tilde{d}' e^{i\tilde{\theta}'} = \zeta' d' e^{i\theta'} , \tag{70}$$

where

$$\zeta' \equiv \frac{1 + x'}{1 + r'_{PA}} \quad \text{and} \quad r_{PA} \equiv \frac{P A^{(ct)}}{P^{(ct)}} \tag{71}$$

parametrize the exchange and penguin-annihilation topologies. Neglecting these topologies gives $\zeta' = 1$, leading to a direct relation between the hadronic parameters of $B_d^0 \to \pi^- K^+$ and $B_s^0 \to K^- K^+$. We discuss the parameter ζ' further in Section 6. Non-factorizable contributions to the $SU(3)$ relation in Eq. (69) are expected to be small as the tree and penguin topologies differ only at the spectator-quark level.

In analogy to R_K, we introduce

$$\tilde{R}_K \equiv \frac{\Gamma(B_d \to \pi^- K^+)}{|d\Gamma(B_d^0 \to \pi^- \ell^+ \nu_\ell)/dq^2|_{q^2 = m_K^2}} = 6\pi^2 |V_{us}|^2 f_K^2 \tilde{X}_K \tilde{r}_K |\tilde{a}'_{\rm NF}|^2 , \tag{72}$$

where

$$\tilde{r}_K \equiv 1 + 2\frac{\tilde{d}'}{\epsilon} \cos\tilde{\theta}' \cos\gamma + \left(\frac{\tilde{d}'}{\epsilon}\right)^2 \tag{73}$$

and

$$\tilde{X}_K \equiv \frac{(m_{B_d}^2 - m_\pi^2)^2}{[m_{B_d}^2 - (m_\pi + m_K)^2][m_{B_d}^2 - (m_\pi - m_K)^2]} \left[\frac{F_0^{B_d\pi}(m_K^2)}{F_1^{B_d\pi}(m_K^2)}\right]^2 . \tag{74}$$

The non-factorizable contributions are parametrized by

$$\tilde{a}'_{\rm NF} \equiv (1 + \tilde{r}'_P) \tilde{a}_{\rm NF}^{T\prime} . \tag{75}$$

In analogy to Eq. (56), we can now write

$$\tilde{r}_K = \frac{\tilde{R}_K}{R_\pi} \left(\frac{|V_{ud}| f_\pi}{|V_{us}| f_K}\right)^2 \frac{X_\pi}{\tilde{X}_K} (\tilde{\xi}^a_{\rm NF})^2 (1 - 2d\cos\theta\cos\gamma + d^2) \tag{76}$$

with

$$\tilde{\xi}^a_{\rm NF} \equiv \left|\frac{1+r_P}{1+\tilde{r}'_P}\right| |1+x| \left|\frac{a^T_{\rm NF}}{\tilde{a}^{T'}_{\rm NF}}\right|, \tag{77}$$

where now only a single $|1+x|$ term occurs, which vanishes if the E and PA topologies are neglected. Interestingly, the semileptonic decay rates cancel in the ratio $\tilde{R}_K/R_\pi$ up to small corrections due to the difference in the corresponding kinematical points.

The direct CP asymmetry of $B^0_d \to \pi^- K^+$ has been measured as follows [20]:

$$\mathcal{A}^{\rm dir}_{\rm CP}(B_d \to \pi^- K^+) \equiv \frac{|A(B^0_d \to \pi^- K^+)|^2 - |A(\bar{B}^0_d \to \pi^+ K^-)|^2}{|A(B^0_d \to \pi^- K^+)|^2 + |A(\bar{B}^0_d \to \pi^+ K^-)|^2} = 0.082 \pm 0.006\,. \tag{78}$$

From the current data for the $B^0_d \to \pi^-\pi^+$ CP asymmetries, using also $\gamma = (70 \pm 7)^\circ$ and $\phi_d = (43.2 \pm 1.8)^\circ$ as input, we find

$$d = 0.58 \pm 0.16\,, \qquad \theta = (151.4 \pm 7.6)^\circ\,. \tag{79}$$

Neglecting the E and PA topologies and applying the U-spin symmetry for $\tilde{\xi}^a_{\rm NF}$, we obtain $\tilde{r}_K$. Combined with the direct CP asymmetry for $B^0_d \to \pi^- K^+$ this gives

$$\tilde{d}' = 0.50 \pm 0.03\,, \qquad \tilde{\theta}' = (157.2 \pm 2.2)^\circ\,. \tag{80}$$

Moreover, we can also determine the results

$$\tilde{\xi} \equiv \tilde{d}'/d = 0.87 \pm 0.20, \qquad \tilde{\Delta} \equiv \tilde{\theta}' - \theta = (5.8 \pm 8.3)^\circ\,, \tag{81}$$

which are fully consistent with the U-spin symmetry. In particular, the anomalously large U-spin-breaking corrections of (50–100)% considered in Ref. [8] are strongly disfavoured.

Finally, we determine the hadronic phase shift as follows:

$$\Delta\phi_{KK} = -(10.8 \pm 0.6)^\circ. \tag{82}$$

Already this precision for the current data is impressive and shows the exciting prospects for the method. Using the current data for the $B^0_s \to K^- K^+$ CP asymmetries, which yield $\phi^{\rm eff}_s = -(17.6 \pm 7.9)^\circ$, we obtain

$$\phi_s = -(6.8 \pm 7.9)^\circ, \tag{83}$$

where the uncertainty is dominated by the experimental data. This value is in excellent agreement with the result in Eq. (30), although obtained with a completely different method. As we have neglected the exchange and penguin-annihilation contributions, this agreement indicates that these topologies are actually playing a minor role.

4.4 News from LHCb

The LHCb collaboration has recently reported new preliminary measurements of the CP-violating observables of the $B^0_s \to K^- K^+$ and $B^0_d \to \pi^-\pi^+$ decays [55]. We have summarized these results in Table 3. Comparing to the experimental data for the CP asymmetries in Table 1, which includes also our scenario for the LHCb upgrade, we find good agreement for the $B^0_d \to \pi^-\pi^+$ channel.

However, while the mixing-induced CP asymmetry of $B^0_s \to K^- K^+$ is also in good agreement with the numbers in this table, the new measurement of the direct CP asymmetry is surprising. In particular, there is a large difference between the direct CP

Observable	Measurement
$\mathcal{A}_{\rm CP}^{\rm dir}(B_d \to \pi^-\pi^+)$	-0.24 ± 0.07
$\mathcal{A}_{\rm CP}^{\rm mix}(B_d \to \pi^-\pi^+)$	0.68 ± 0.06
$\mathcal{A}_{\rm CP}^{\rm dir}(B_s \to K^-K^+)$	0.24 ± 0.06
$\mathcal{A}_{\rm CP}^{\rm mix}(B_s \to K^-K^+)$	-0.22 ± 0.06
$\mathcal{A}_{\Delta\Gamma}(B_s \to K^-K^+)$	-0.75 ± 0.13

Table 3: Overview of the preliminary new LHCb measurements [55].

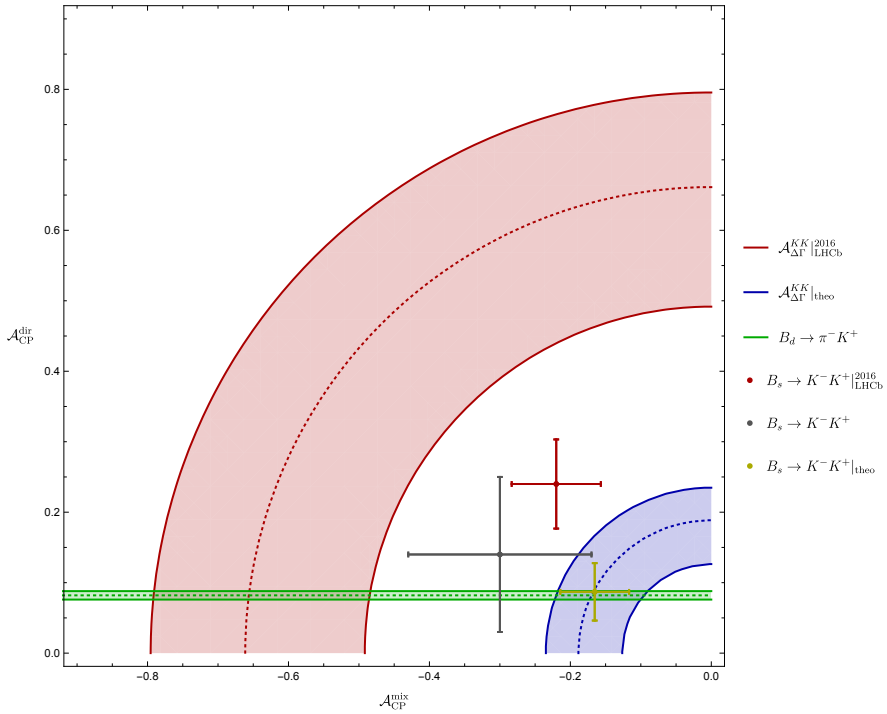

Figure 7: Comparison of the new LCHb data with the previous results and theoretically predicted values for the $B_s^0 \to K^-K^+$ CP asymmetries, as discussed in the text. Moreover, we show contours corresponding to the new and predicted values of $\mathcal{A}_{\Delta\Gamma}(B_s^0 \to K^-K^+)$ as well as the current direct CP asymmetry of $B_d^0 \to \pi^-K^+$.

asymmetry of $B_s^0 \to K^-K^+$ in Table 3 and the direct CP asymmetry of $B_d^0 \to \pi^-K^+$ in Eq. (78). As we discussed in the previous section, these decays differ only through their spectator quarks. Since the underlying quark-level transitions are the same, NP effects cannot be responsible for this difference. As exchange and penguin-annihilation topologies contribute to the $B_s^0 \to K^-K^+$ decay but have no counterparts in the $B_d^0 \to \pi^-K^+$ mode, they could – in principle – be the origin of this surprising measurement. However, as we will show in detail in Sections 5 and 6, such a picture is not supported by experimental data. Moreover, a similar relation arises between the direct CP asymmetries of the $B_d^0 \to \pi^-\pi^+$ and $B_s^0 \to K^-\pi^+$ decays, which is perfectly satisfied by the data, thereby also not indicating any anomalous behaviour.

In combination with the CP asymmetries, the LHCb collaboration has also reported a new preliminary measurement of the observable $\mathcal{A}_{\Delta\Gamma}^{KK} \equiv \mathcal{A}_{\Delta\Gamma}(B_s \to K^-K^+)$ [55], which we give in Table 3. An important check for the internal consistency of the data is provided by the sum rule in Eq. (15), which is a general feature of the different observables and

cannot be violated through NP effects. For the preliminary LHCb data, we find the following result:

$$\Delta_{\rm SR} \equiv 1 - \left(\mathcal{A}_{\rm CP}^{\rm dir\,\prime}\right)^2 - \left(\mathcal{A}_{\rm CP}^{\rm mix\prime}\right)^2 - \left(\mathcal{A}_{\Delta\Gamma}^{KK}\right)^2 = 0.33 \pm 0.20\,, \tag{84}$$

which differs from zero at the $1.7\,\sigma$ level. We have illustrated this situation in Fig. 7, where we indicate the CP asymmetries of $B_s^0 \to K^-K^+$ from Table 1 and the preliminary new results listed in Table 3 through grey and red data points, respectively. Moreover, we add a red circular band corresponding to Eq. (84), which clearly shows the inconsistency of the data. In Fig. 7, we have furthermore considered predictions of the $B_s^0 \to K^-K^+$ CP asymmetries and $\mathcal{A}_{\Delta\Gamma}^{KK}$, calculated from Eqs. (12), (13) and (14) by applying the U-spin symmetry to d and θ from Eq. (79), which lead to the yellow data point and the blue circular band, respectively. They are in perfect agreement with the direct CP asymmetry of $B_d^0 \to \pi^-K^+$ represented by the green horizontal band. We expect that the central value of the new LHCb result for the direct CP asymmetry of the $B_s^0 \to K^-K^+$ decay will move correspondingly in the future.

5 Insights into Penguin Dynamics

The size of the parameters r_P and x introduced in Eq. (48) has to be quantified in order to analyze the theoretical precision of our strategy in more detail. In this section, we discuss the penguin topologies contributing to r_P. Specifically, we write

$$1 + r_P = \frac{1}{1 - \zeta d e^{i\theta}\rho_P}\,, \tag{85}$$

where the penguin ratio ρ_P is defined as

$$\rho_P \equiv |\rho_P| e^{i\theta_P} = R_b \frac{P^{(ut)}}{P^{(ct)}}\,, \tag{86}$$

and

$$\zeta \equiv |\zeta| e^{i\omega} = \frac{1+x}{1+r_{PA}}\,, \qquad r_{PA} \equiv \frac{PA^{(ct)}}{P^{(ct)}}\,. \tag{87}$$

Completely analogous expressions hold for $1 + r_P'$.

The parameter ζ' was already introduced in Eq. (70), and $\zeta^{(\prime)}$ is expected to be close to one as the exchange and penguin-annihilation topologies are expected to be small. We shall return to this quantity in Section 6. Let us first focus on the parameter ρ_P, which is governed by the interplay of the QCD penguin topologies with internal up, charm and top quarks [56]. This quantity can be studied with the pure penguin decays $B_d^0 \to K^0\overline{K}^0$, $B_d^0 \to K^0\overline{K}^0$ and $B^+ \to K^+\overline{K}^0$, $B^+ \to \pi^+K^0$. The various decay topologies and their specific use in our new strategy are summarized in Table 5. In Subsection 5.3, we shall also discuss the $B_d^0 \to \pi^-K^+$, $B_s^0 \to K^-\pi^+$ system [57], which has only tree and penguin contributions and can hence also be used to study U-spin-breaking effects in the corresponding decay topologies.

5.1 $B_d^0 \to K^0\overline{K}^0$ and $B_s^0 \to K^0\overline{K}^0$

The decays $B_d^0 \to K^0\overline{K}^0$ and $B_s^0 \to K^0\overline{K}^0$ are related by the U-spin symmetry and receive only contributions from penguin and penguin annihilation topologies [58, 59]. Consequently, they offer an excellent laboratory to study penguin contributions.

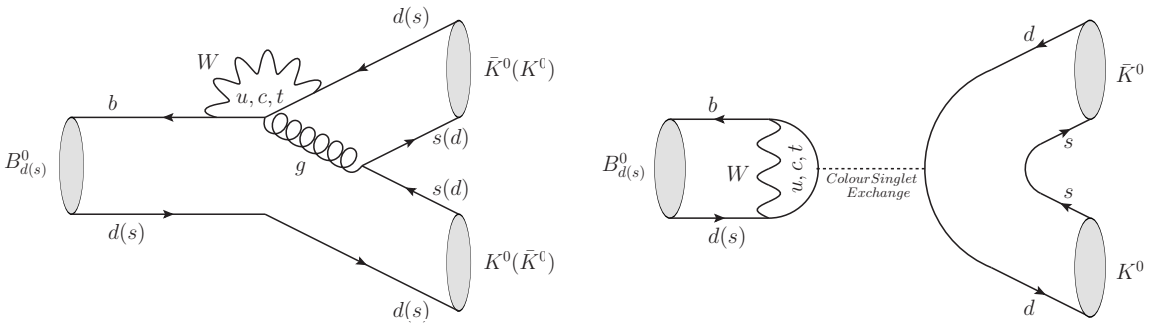

(a) QCD penguin (P_{KK}) (b) Penguin annihilation (PA_{KK})

Figure 8: Topologies of the $B^0_d \to K^0\overline{K}^0$ and $B^0_s \to K^0\overline{K}^0$ decays.

As can be seen in Fig. 8, the penguin topologies of $B^0_d \to K^0\overline{K}^0$ and $B^0_s \to K^0\overline{K}^0$ differ from those of $B^0_d \to \pi^-\pi^+$ and $B^0_s \to K^-K^+$ only through the quark pair that is generated by the gluon. Consequently, the $B^0_{d,s} \to K^0\overline{K}^0$ system offers the most suitable probes for ρ_P and subsequently r_P. We shall neglect tiny contributions from colour-suppressed electroweak penguins.

The corresponding decay amplitudes can be written as [60]

$$\begin{aligned} A(B^0_d \to K^0\overline{K}^0) &= -\mathcal{C}_{KK}\left[1 - d_{KK}e^{i\theta_{KK}}e^{i\gamma}\right], \\ A(B^0_s \to K^0\overline{K}^0) &= \frac{1}{\sqrt{\epsilon}}\mathcal{C}'_{KK}\left[1 + \epsilon d'_{KK}e^{i\theta'_{KK}}e^{i\gamma}\right], \end{aligned} \tag{88}$$

with

$$\mathcal{C}_{KK} \equiv A\lambda^3\left[P^{(ct)}_{KK} + PA^{(ct)}_{KK}\right], \qquad d_{KK}e^{i\theta_{KK}} \equiv R_b\left[\frac{P^{(ut)}_{KK} + PA^{(ut)}_{KK}}{P^{(ct)}_{KK} + PA^{(ct)}_{KK}}\right], \tag{89}$$

and analogous expressions for $\mathcal{C}'_{KK}$ and $d'_{KK}e^{i\theta'_{KK}}$. In contrast to ρ_P, the parameter $d_{KK}e^{i\theta_{KK}}$ also receives contributions from PA topologies. However, these topologies are suppressed in comparison with the leading penguin contributions and can therefore be neglected. Since the decays $B^0_d \to K^0\overline{K}^0$, $B^0_s \to K^0\overline{K}^0$ and $B^0_d \to \pi^-\pi^+$, $B^0_s \to K^-K^+$ are related to one another by the $SU(3)$ flavour symmetry, the extraction of $d^{(\prime)}_{KK}e^{i\theta^{(\prime)}_{KK}}$ allows a determination of $\rho^{(\prime)}_P$.

The CP asymmetries are given as follows:

$$\begin{aligned} \mathcal{A}^{\rm dir}_{\rm CP}(B_d \to K^0\overline{K}^0) &= \frac{2d_{KK}\sin\theta_{KK}\sin\gamma}{1 - 2d_{KK}\cos\theta_{KK}\cos\gamma + d^2_{KK}}, \\ \mathcal{A}^{\rm mix}_{\rm CP}(B_d \to K^0\overline{K}^0) &= \frac{\sin\phi_d - 2d_{KK}\cos\theta_{KK}\sin(\phi_d+\gamma) + d^2_{KK}\sin(\phi_d+2\gamma)}{1 - 2d_{KK}\cos\theta_{KK}\cos\gamma + d^2_{KK}}, \end{aligned} \tag{90}$$

with analogous "primed" expressions for the CP asymmetries of $B^0_s \to K^0\overline{K}^0$. The CP asymmetries of $B^0_d \to K^0\overline{K}^0$ have been measured by the BaBar [61] and Belle collaborations [62]. We list them in Table 4, together with their PDG average [30]. The experimental situation is not conclusive and will hopefully be settled with future data.

If we use the mixing phases $\phi_{d,s}$ as input, the experimental results for these CP asymmetries can be converted into theoretically clean values of the parameters $d_{KK}e^{i\theta_{KK}}$ and $d'_{KK}e^{i\theta'_{KK}}$, which will allow valuable insights into the dynamics of penguin topologies,

CP asymmetry	BaBar [61]	Belle [62]	PDG [30]
$\mathcal{A}_{\rm CP}^{\rm dir}(B_d \to K^0\overline{K}^0)$	$-0.40 \pm 0.41 \pm 0.06$	$0.38 \pm 0.38 \pm 0.05$	0.0 ± 0.4
$\mathcal{A}_{\rm CP}^{\rm mix}(B_d \to K^0\overline{K}^0)$	$1.28 \pm 0.80 \pm 0.16$	$0.38 \pm 0.77 \pm 0.09$	0.8 ± 0.5

Table 4: Overview of the $B_d^0 \to K^0\overline{K}^0$ CP asymmetries, where we have conservatively taken the largest uncertainty if the error was asymmetric.

shedding light on the issue of the "charming penguins" and into U-spin-breaking effects in these penguin parameters. As form factors cancel, those effects are genuinely related to non-factorizable effects. Using the $SU(3)$ flavour symmetry to relate the hadronic parameters of the $B_s^0 \to K^0\overline{K}^0$, $B_d^0 \to K^0\overline{K}^0$ system to those of the $B_d^0 \to \pi^-\pi^+$, $B_s^0 \to K^-K^+$ modes allows the determination of both ρ_P and ρ'_P.

Since there is currently no measurement of the CP asymmetries in $B_s^0 \to K^0\overline{K}^0$, we consider the following ratio of branching ratios:

$$\begin{aligned} H_{KK} &\equiv \frac{1}{\epsilon}\left|\frac{\mathcal{C}'_{KK}}{\mathcal{C}_{KK}}\right|^2 \left[\frac{m_{B_d}}{m_{B_s}}\frac{\Phi(m_K/m_{B_s}, m_K/m_{B_s})}{\Phi(m_K/m_{B_d}, m_K/m_{B_d})}\frac{\tau_{B_s}}{\tau_{B_d}}\right] \frac{\mathcal{B}(B_d \to K^0\overline{K}^0)}{\mathcal{B}(B_s \to K^0\overline{K}^0)} \\ &= \frac{1 - 2d_{KK}\cos\theta_{KK}\cos\gamma + d_{KK}^2}{1 + 2\epsilon d'_{KK}\cos\theta'_{KK}\cos\gamma + \epsilon^2 d'^2_{KK}} \ , \end{aligned} \tag{91}$$

where the phase-space function Φ was introduced in Eq. (25). The various measurements of the $B_d^0 \to K^0\overline{K}^0$ branching ratio are consistent with one another, and the PDG average [30] reads

$$\mathcal{B}(B_d^0 \to K^0\overline{K}^0) = (1.21 \pm 0.16) \times 10^{-6}. \tag{92}$$

The Belle collaboration has recently announced the observation of the $B_s^0 \to K^0\overline{K}^0$ channel [63], resulting in the branching ratio

$$\mathcal{B}(B_s^0 \to K^0\overline{K}^0) = (19.6^{+6.2}_{-5.6}) \times 10^{-6} \ . \tag{93}$$

Using the factorization approximation, we obtain

$$\left|\frac{\mathcal{C}'_{KK}}{\mathcal{C}_{KK}}\right|_{\rm fact} = \left(\frac{m_{B_s}^2 - m_K^2}{m_{B_d}^2 - m_K^2}\right)\left[\frac{F_0^{B_sK}(m_K^2)}{F_0^{B_dK}(m_K^2)}\right] = 0.92 \pm 0.13, \tag{94}$$

where we have used LCSR results for the corresponding form factors [23]. Using the information for the branching ratios then gives

$$H_{KK} = 0.94 \ \pm 0.13|_{B_d} \ \pm 0.29|_{B_s} \ \pm 0.27|_{\mathcal{C}} = 0.94 \pm 0.42, \tag{95}$$

where we show the individual contributions of the various quantities to the error budget.

If we apply the U-spin relation

$$d_{KK}e^{i\theta_{KK}} = d'_{KK}e^{i\theta'_{KK}}, \tag{96}$$

the observable H_{KK} and the CP asymmetries of the $B_d \to K^0\overline{K}^0$ channel allow the extraction of γ and the hadronic parameters [58]; further information can be obtained through the measurement of CP violation in $B_s^0 \to K^0\overline{K}^0$. However, due to the large current uncertainties for both the CP asymmetries of $B_d^0 \to K^0\overline{K}^0$ and the observable H_{KK} only very weak constraints can be obtained.

5.2 $B^+ \to K^+\overline{K}^0$ and $B^+ \to \pi^+ K^0$

Given the current experimental results for the $B_d^0 \to K^0\overline{K}^0$, $B_s^0 \to K^0\overline{K}^0$ system discussed in the previous subsection, the charged $B^+ \to K^+\overline{K}^0$, $B^+ \to \pi^+ K^0$ decays offer an interesting alternative. These modes were previously studied in Ref. [5]. Let us update this analysis using the current data. The decays $B^+ \to K^+\overline{K}^0$ and $B^+ \to \pi^+ K^0$ are characterized by $\bar{b} \to \bar{s}s\bar{d}$ and $\bar{b} \to \bar{d}d\bar{s}$ transitions, respectively, and related to each other by the U-spin symmetry. The $B^+ \to K^+\overline{K}^0, B^+ \to \pi^+ K^0$ modes can be related to the $B_d^0 \to K^0\overline{K}^0$, $B_s^0 \to K^0\overline{K}^0$ decays by applying the $SU(3)$ flavour symmetry at the spectator-quark level, thereby allowing us to determine ρ_P.

The corresponding decay amplitudes can be written in the following form [5]:

$$A(B^+ \to \pi^+ K^0) = \mathcal{P}_{\pi K}\left[1 + \epsilon\rho_{\pi K} e^{i\sigma_{\pi K}} e^{i\gamma}\right] \tag{97}$$

$$A(B^+ \to K^+\overline{K}^0) = \sqrt{\epsilon}\mathcal{P}_{KK}\left[1 - \rho_{KK} e^{i\sigma_{KK}} e^{i\gamma}\right] \ , \tag{98}$$

where

$$\rho_{\pi K} e^{i\sigma_{\pi K}} \equiv R_b \frac{\mathcal{P}^{(ut)\prime}}{\mathcal{P}^{(ct)\prime}} \ , \tag{99}$$

and in analogy

$$\rho_{KK} e^{i\sigma_{KK}} \equiv R_b \frac{\mathcal{P}^{(ut)}}{\mathcal{P}^{(ct)}}. \tag{100}$$

The CP asymmetry is defined by

$$\begin{aligned} \mathcal{A}_{\rm CP}^{\rm dir}(B^\pm \to \pi^\pm K) &\equiv \frac{|A(B^+ \to \pi^+ K^0)|^2 - |A(B^- \to \pi^- \overline{K}^0)|^2}{|A(B^+ \to \pi^+ K^0)|^2 + |A(B^- \to \pi^- \overline{K}^0)|^2} \\ &= \frac{-2\epsilon\rho_{\pi K}\sin\sigma_{\pi K}\sin\gamma}{1 + 2\epsilon\rho_{\pi K}\cos\sigma_{\pi K}\cos\gamma + \epsilon^2\rho_{\pi K}^2} \ , \end{aligned} \tag{101}$$

while the expression for the direct CP asymmetry of $B^+ \to K^+\overline{K}^0$ can be obtained straightforwardly by making the following replacements:

$$\epsilon \to -1 \ , \quad \rho_{\pi K} \to \rho_{KK} \ , \quad \sigma_{\pi K} \to \sigma_{KK} \ . \tag{102}$$

The experimental averages for the direct CP asymmetry are given by HFAG [20] as

$$\begin{aligned} \mathcal{A}_{\rm CP}^{\rm dir}(B^\pm \to \pi^\pm K) &= 0.017 \pm 0.016 \ , \\ \mathcal{A}_{\rm CP}^{\rm dir}(B^\pm \to K^\pm K) &= 0.087 \pm 0.100 \ , \end{aligned} \tag{103}$$

while the branching ratios are listed in Table 2. We note that both CP asymmetries have switched signs with respect to their values in 2007 [5].

As before, we introduce

$$\begin{aligned} H_{\pi K}^{KK} &\equiv \frac{1}{\epsilon}\left|\frac{\mathcal{P}_{\pi K}}{\mathcal{P}_{KK}}\right|^2 \left[\frac{\Phi(m_\pi/m_B, m_K/m_B)}{\Phi(m_K/m_B, m_K/m_B)}\right] \frac{\mathcal{B}(B^\pm \to K^\pm K)}{\mathcal{B}(B^\pm \to \pi^\pm K)} \ , \\ &= \frac{1 - 2\rho_{KK}\cos\sigma_{KK}\cos\gamma + \rho_{KK}^2}{1 + 2\epsilon\rho_{\pi K}\cos\sigma_{\pi K}\cos\gamma + \epsilon^2\rho_{\pi K}^2} = 0.57 \pm 0.11 \ , \end{aligned} \tag{104}$$

where we used the following result arising within factorization [23]:

$$\left|\frac{\mathcal{P}_{KK}}{\mathcal{P}_{\pi K}}\right|_{\rm fact} = \left[\frac{m_B^2 - m_K^2}{m_B^2 - m_\pi^2}\right]\left[\frac{F_0^{BK}(m_K^2)}{F_0^{B\pi}(m_K^2)}\right] = 1.35 \pm 0.11 \ . \tag{105}$$

Combining the CP asymmetries of $B^+ \to K^+\overline{K}^0$ and $B^+ \to \pi^+ K^0$ with $H_{\pi K}^{KK}$, and assuming the U-spin relation

$$\rho_{KK} = \rho_{\pi K} \qquad \sigma_{KK} = \sigma_{\pi K} \ , \tag{106}$$

we find the constraints for ρ_{KK} and σ_{KK} shown in Fig. 9, which were obtained through a χ^2-minimalization fit where also $\gamma = (70 \pm 7)^\circ$ was added as a constraint. The best fit result favours interestingly a smaller value of $\gamma = 60^\circ$, which is caused by the small value of $H_{\pi K}$. This feature has already been noted in Ref. [5]. Assuming Gaussian distributions, we obtain from the fit

$$\rho_{KK} = 0.52 \pm 0.2 \ , \qquad \sigma_{KK} = (2.6 \pm 4.6)^\circ \ . \tag{107}$$

These values are in agreement with the estimates in Ref. [56] and the general hierarchy of decay topologies discussed in Refs. [10,11]. We will discuss the implications for $|1+r_P|$ and Ξ_P in Subsection 6.5.

Using the strong isospin symmetry to relate the up spectator quark in $B^+ \to K^+\overline{K}^0$ to the down spectator quark in $B_d^0 \to K^0\overline{K}^0$ gives the relation

$$d_{KK} = \rho_{KK}, \qquad \theta_{KK} = \sigma_{KK} \ . \tag{108}$$

We shall assume these relations, which we expect to hold with excellent precision, for the remainder of this section. Using Eq. (107), we may calculate the CP-violating observables of the $B_d^0 \to K^0\overline{K}^0$ decay:

$$\begin{aligned} \mathcal{A}_{\rm CP}^{\rm mix}(B_d \to K^0\overline{K}^0) &= -0.32 \pm 0.39, \\ \mathcal{A}_{\rm CP}^{\rm dir}(B_d \to K^0\overline{K}^0) \ &= 0.05 \pm 0.09, \end{aligned} \tag{109}$$

where the errors are dominated by the uncertainty of ρ_{KK}. These values are in agreement with the current experimental measurements given in Table 4, although the experimental uncertainties are unfortunately too large to draw any conclusions.

Improved CP violation measurements in $B_d^0 \to K^0\overline{K}^0$ would allow a powerful and theoretically clean determination of ρ_{KK} and σ_{KK}, as illustrated in Fig. 9. Here we have added the contours from the expected CP asymmetries in $B_d^0 \to K^0\overline{K}^0$ with an assumed error of 0.05 in the era of Belle II and the LHCb upgrade. We observe that in particular the mixing-induced CP asymmetry of $B_d^0 \to K^0\overline{K}^0$ has the potential to constrain ρ_{KK} much further, thereby reducing the uncertainty for an important parameter of our strategy. A measurement of the mixing-induced CP asymmetry of $B_d^0 \to K^0\overline{K}^0$ with a precision of 0.1 would allow a determination of ρ_{KK} with a precision of 0.1, which would be a significant improvement over the current precision in Eq. (107).

Using in addition a future measurement of the CP asymmetries of the $B_s^0 \to K^0\overline{K}^0$ channel would allow a clean determination of d'_{KK} and θ'_{KK}, thereby offering an interesting test of the U-spin symmetry in these penguin parameters. The observable H_{KK} is not needed for this analysis, but offers instead further insights into the U-spin symmetry for the QCD penguin topologies.

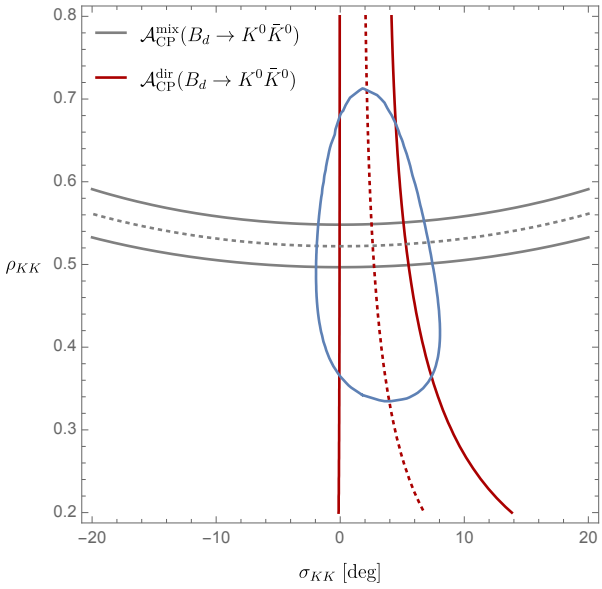

Figure 9: Results from a χ^2-minimalization fit to the current data as described in text. The blue contour shows the 1σ constraint from the fit. The red (gray) contour shows the expected constraint from the direct (mixing-induced) CP asymmetries in $B_d \to K^0\overline{K}^0$ with an anticipated error of 0.05.

5.3 $B_d^0 \to \pi^- K^+$ and $B_s^0 \to K^- \pi^+$

The decays $B_d^0 \to \pi^- K^+$ and $B_s^0 \to K^- \pi^+$ receive only contributions from tree and penguin topologies and are related to each other through the U-spin symmetry [5, 57]. We have already encountered the $B_d^0 \to \pi^- K^+$ channel in Subsection 4.3, while the amplitude for $B_s^0 \to K^- \pi^+$ takes the form

$$A(B_s^0 \to K^-\pi^+) = e^{i\gamma}\tilde{\mathcal{C}}\left[1 - \tilde{d}e^{i\tilde{\theta}}e^{-i\gamma}\right] , \tag{110}$$

where $\tilde{\mathcal{C}}$ and $\tilde{d}e^{i\tilde{\theta}}$ are defined in analogy to Eq. (68).

As the final states are flavour-specific, only direct CP violation can occur. The expressions for the direct CP asymmetry can be obtained by making suitable replacements in Eq. (12). The current direct CP asymmetries as given by the PDG are [30]:

$$\mathcal{A}_{CP}^{dir}(B_d^0 \to \pi^- K^+) = 0.082 \pm 0.006 \quad (0.082 \pm 0.003) , \tag{111a}$$

$$\mathcal{A}_{CP}^{dir}(B_s^0 \to K^- \pi^+) = -0.26 \pm 0.035 \quad (-0.26 \pm 0.006) . \tag{111b}$$

In parentheses, we give a future scenario for the Belle II and LHCb upgrade era [2, 3].

For the current data, the CP asymmetries combined with the U-spin relation

$$\tilde{d}e^{i\tilde{\theta}} = \tilde{d}'e^{i\tilde{\theta}'} \tag{112}$$

give the constraints for $(\tilde{d}, \tilde{\theta})$ shown in Fig. 10. They are obtained using a χ^2 fit with $\gamma = (70 \pm 7)^\circ$ added as a constraint. We find

$$\tilde{d} = 0.54 \pm 0.06 , \qquad \tilde{\theta} = (155.4 \pm 3.3)^\circ . \tag{113}$$

For the upgrade scenario in Eq. (111) with $\gamma = (70 \pm 1)^\circ$, the fit gives

$$\tilde{d} = 0.54 \pm 0.02 , \qquad \tilde{\theta} = (155.4 \pm 0.6)^\circ . \tag{114}$$

These determinations agree with the picture arising from CP violation in $B_d^0 \to \pi^-\pi^+$ and the values in Eq. (80). Specifically, the parameter

$$\zeta \equiv |\zeta| e^{i\omega} \tag{115}$$

relates the hadronic parameters. Using Eq. (42), we find for the upgrade scenario

$$|\zeta| \equiv \tilde{d}/d = 0.93 \pm 0.05 \;, \qquad \omega \equiv \tilde{\theta} - \theta = (4.0 \pm 1.3)^\circ \;, \tag{116}$$

showing an impressive accuracy for the picture assumed in the era of Belle II and the LHCb upgrade.

Let us now utilize again the information provided by semileptonic decays. In order to complement the ratio $\tilde{R}_K$ defined in Eq. (72), we introduce

$$\tilde{R}'_K \equiv \frac{\Gamma(B_s^0 \to K^-\pi^+)}{d\Gamma(B_s^0 \to K^-\ell^+\nu_\ell)/dq^2|_{q^2=m_\pi^2}} \;, \tag{117}$$

which requires the measurement of the semileptonic differential rate of the decay $B_s^0 \to K^-\ell^+\nu_\ell$, which we require also for our key observable R_K. In analogy to our new strategy, we may determine the parameters $\tilde{d}, \tilde{\theta}$ and $\tilde{d}', \tilde{\theta}'$, which allow an interesting test of the U-spin symmetry in the dominant tree and penguin topologies.

Lacking at the moment a measurement of $B_s^0 \to K^-\ell^+\nu_\ell$, we might also consider the ratio of branching ratios, as we discussed for the $B_d^0 \to \pi^-\pi^+$, $B_s^0 \to K^-K^+$ system:

$$\begin{aligned}\tilde{K} &\equiv \frac{1}{\epsilon}\left|\frac{\tilde{\mathcal{C}}}{\tilde{\mathcal{C}}'}\right|^2 \left[\frac{m_{B_d}}{m_{B_s}}\frac{\Phi(m_{K^\pm}/m_{B_s}, m_{\pi^\pm}/m_{B_s})}{\Phi(m_{\pi^\pm}/m_{B_d}, m_{K^\pm}/m_{B_d})}\frac{\tau_{B_s}}{\tau_{B_d}}\right] \frac{\mathcal{B}(B_d \to \pi^-K^+)}{\mathcal{B}(B_s \to K^-\pi^+)_{\rm theo}}, \\ &= \frac{1 + 2(\tilde{d}'/\epsilon)\cos\tilde{\theta}'\cos\gamma + (\tilde{d}'/\epsilon)^2}{1 - 2\tilde{d}\cos\tilde{\theta}\cos\gamma + \tilde{d}^2} \stackrel{\rm exp}{=} 63.6^{+20.1}_{-12.3} \;,\end{aligned} \tag{118}$$

where we used the factorization approximation to obtain

$$\left|\frac{\tilde{\mathcal{C}}}{\tilde{\mathcal{C}}'}\right|_{\rm fact} = \frac{f_\pi}{f_K}\left[\frac{m_{B_s}^2 - m_K^2}{m_{B_d}^2 - m_\pi^2}\right]\left[\frac{F_0^{B_sK}(m_\pi^2)}{F_0^{B_d\pi}(m_K^2)}\right] = 0.99^{+0.15}_{-0.08} \;. \tag{119}$$

The ratio of form factors $F_0^{B_sK}(0)/F_0^{B_d\pi}(0) = 1.15^{+0.17}_{-0.09}$ follows from an LCSR calculation [22], and $f_K/f_\pi = 1.1928 \pm 0.0026$ [24]. It is interesting to note that the form factors and decay constants enter Eq. (119) in such a way that they almost cancel.

The uncertainty of Eq. (118) is dominated by the form factors. If we assume a perfect determination of $|\tilde{\mathcal{C}}/\tilde{\mathcal{C}}'| = 1$, we find $\tilde{K} = 65.1 \pm 7.3$. Combining the ratio $\tilde{K}$ with $\gamma = (70 \pm 7)^\circ$ gives an additional constraint on $(\tilde{d}, \tilde{\theta})$, which we have added to Fig. 10. There, the wide band and central value follow from Eq. (118), while the small band corresponds to the situation for $|\tilde{\mathcal{C}}/\tilde{\mathcal{C}}'| = 1$. We find good agreement with the constraints following from the measurements of direct CP violation in the $B_d^0 \to \pi^-K^+$ and $B_s^0 \to K^-\pi^+$ decays, which we also give in Fig. 10. The latter are not affected by form factor uncertainties. The consistent picture in Fig. 10 is remarkable and does not point towards any anomalously large U-spin-breaking effects.

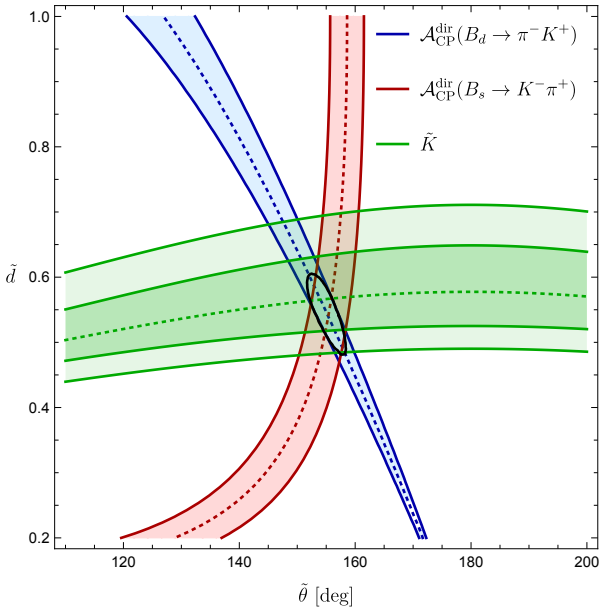

Figure 10: Current constraints on the penguin parameters $\tilde{d}$ and $\tilde{\theta}$ from the $B_d^0 \to \pi^- K^+$, $B_s^0 \to K^- \pi^+$ CP asymmetries and ratio $\tilde{K}$. The black contour gives the constraints from a χ^2 fit to the CP asymmetries and $\gamma = (70 \pm 7)^\circ$. For $\tilde{K}$, we consider $|\tilde{\mathcal{C}}/\tilde{\mathcal{C}}'|$ in factorization (wide band) and $|\tilde{\mathcal{C}}/\tilde{\mathcal{C}}'| = 1$ (small band).

6 Insights into Exchange and Penguin Annihilation Dynamics

The exchange and penguin annihilation contributions enter our new strategy through the parameter $\xi_{\rm NF}^a$. Consequently, we need information about these topologies to assess the theoretical precision. Specifically, we study the parameters x (see Eq. (48)) and ζ (see Eq. (87)) and their U-spin partners, which enter Ξ_x and Ξ_P, respectively. Fortunately, we may use experimental data to determine the size of these contributions and do not have to rely on model-dependent assumptions. In Table 5, we give an overview of the relevant $B \to hh$ decays ($h = \pi, K$) and the topologies that are used to obtain insights into the different contributions to our strategy.

The $B_d^0 \to K^- K^+$ and $B_s^0 \to \pi^- \pi^+$ modes emerge only from exchange and penguin-annihilation topologies. Consequently, this allows us to explore these contributions in a direct way. Unfortunately, the current experimental data is not yet sufficient to make full use of the potential of these decays although important constraints can already be obtained, with excellent future prospects. In view of this situation, we discuss also alternative indirect determinations of the exchange and penguin-annihilation topologies in Subsections 6.2 and 6.3. In Subsection 6.4, we return to the $B_d^0 \to K^- K^+$ and $B_s^0 \to \pi^- \pi^+$ decays, discussing future scenarios for the era of Belle II and the LHCb upgrade.

Decay	$\mathcal{C}$	Topologies				Specific use:
		T	P	E	PA	
$B_d^0 \to \pi^-\pi^+$	$\mathcal{C}$	x	x	x	x	Determine d and θ (γ and ϕ_d as input)
$B_d^0 \to \pi^- K^+$	$\tilde{\mathcal{C}}'$	x	x			Direct determination of $T+P$
$B_d^0 \to K^- K^+$	$\hat{\mathcal{C}}$			x	x	Direct determination of E+PA
$B_s^0 \to K^- K^+$	$\mathcal{C}'$	x	x	x	x	Determination of ϕ_s, d', θ'
$B_s^0 \to K^-\pi^+$	$\tilde{\mathcal{C}}$	x	x			Non-factorizable effects in T and P
$B_s^0 \to \pi^-\pi^+$	$\hat{\mathcal{C}}'$			x	x	Non-factorizable effects in E and PA
$B_d^0 \to K^0\overline{K}^0$	$\mathcal{C}_{KK}$		x		x	Direct determination of penguin ratio ρ_P
$B_s^0 \to K^0\overline{K}^0$	$\mathcal{C}'_{KK}$		x		x	Non-factorizable effects in penguin ratio ρ_P
$B^+ \to \pi^+ K^0$	$\mathcal{P}_{\pi K}$		x			Alternative determination of ρ_P
$B^+ \to K^+\overline{K}^0$	$\mathcal{P}_{KK}$		x			Alternative determination of ρ_P

Table 5: Compilation of various $B \to hh$ channels ($h = \pi, K$) with their decay topologies and their use in the context of our strategy.

6.1 Direct Determination from $B_d^0 \to K^-K^+$ and $B_s^0 \to \pi^-\pi^+$

The decays $B_d^0 \to K^-K^+$ and $B_s^0 \to \pi^-\pi^+$ receive only contributions from exchange and penguin annihilation topologies. Their amplitudes are given by

$$A(B_d^0 \to K^-K^+) = e^{i\gamma}\hat{\mathcal{C}}\left[1 - \hat{d}e^{i\hat{\theta}}e^{-i\gamma}\right] \tag{120}$$

$$A(B_s^0 \to \pi^-\pi^+) = \sqrt{\epsilon}e^{i\gamma}\hat{\mathcal{C}}'\left[1 + \frac{1}{\epsilon}\hat{d}'e^{i\hat{\theta}'}e^{-i\gamma}\right] , \tag{121}$$

with

$$\hat{\mathcal{C}} \equiv \lambda^3 A R_b\left[\hat{E} + \hat{PA}^{(ut)}\right] , \qquad \hat{d}e^{i\hat{\theta}} \equiv \frac{1}{R_b}\left[\frac{\hat{PA}^{(ct)}}{\hat{E} + \hat{PA}^{(ut)}}\right] . \tag{122}$$

The parameters $\hat{\mathcal{C}}'$ and $\hat{d}'$ are given by analogous expressions. The CP asymmetries can be obtained from Eq. (12) by replacing $d(\theta) \to \hat{d}(\hat{\theta})$ and equivalently $d'(\theta') \to \hat{d}'(\hat{\theta}')$. Since these CP asymmetries have not yet been measured, we explore the currently available information by considering

$$\begin{aligned}\hat{K} &= \frac{1}{\epsilon}\left|\frac{\hat{\mathcal{C}}}{\hat{\mathcal{C}}'}\right|^2\left[\frac{m_{B_s}}{m_{B_d}}\frac{\Phi(m_K/m_{B_d}, m_K/m_{B_d})}{\Phi(m_\pi/m_{B_s}, m_\pi/m_{B_s})}\frac{\tau_{B_d}}{\tau_{B_s}}\right]\frac{\mathcal{B}(B_s \to \pi^-\pi^+)_{\rm theo}}{\mathcal{B}(B_d \to K^-K^+)} \\ &= \frac{1}{\epsilon^2}\frac{\epsilon^2 + 2\epsilon\hat{d}'\cos\hat{\theta}'\cos\gamma + \hat{d}'^2}{1 - 2\hat{d}\cos\hat{\theta}\cos\gamma + \hat{d}^2} \stackrel{\rm exp}{=} 224.6 \pm 50.2 ,\end{aligned} \tag{123}$$

where we have used the scaling factor [12]

$$\frac{\hat{\mathcal{C}}}{\hat{\mathcal{C}}'} \approx \frac{f_{B_d} f_{K^\pm}^2}{f_{B_s} f_{\pi^\pm}^2} \tag{124}$$

with $f_{B_s}/f_{B_d} = 1.192 \pm 0.006$ [24]. Since there is no effective lifetime measurement for $B_s^0 \to \pi^-\pi^+$ available, we used the experimental branching ratio for simplicity. A more sophisticated analysis can be performed by using the expression of $\mathcal{A}_{\Delta\Gamma}(B_s \to \pi^-\pi^+)$

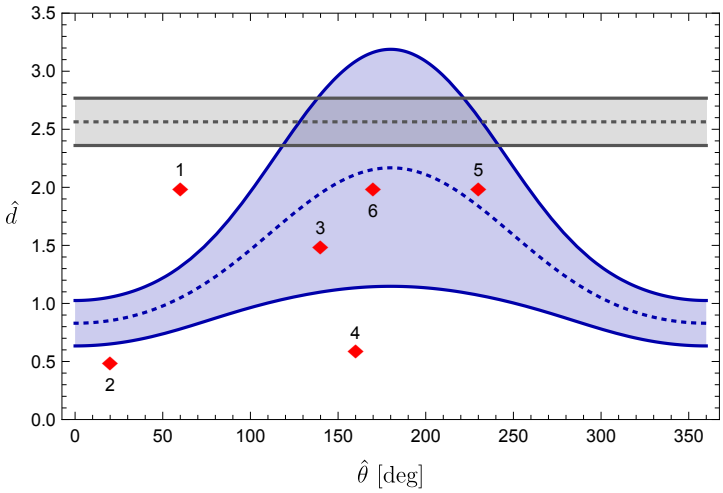

Figure 11: Current constraints on $\hat{d}$ as a function of $\hat{\theta}$. The horizontal band gives the naive constraint on $\hat{d}$ in Eq. (127), discussed in the text. The various diamond points represent the different future scenarios discussed in Section 6.

in terms of the hadronic parameters to convert the experimental into the theoretical branching ratio, applying the formulae given in Subsection 2.3.

Assuming the U-spin relation

$$\hat{d}e^{i\hat{\theta}} = \hat{d}'e^{i\hat{\theta}'} \tag{125}$$

gives

$$\hat{d} = \frac{\epsilon}{1-\epsilon^2\hat{K}}\left[-\cos\hat{\theta}\cos\gamma\left(1+\epsilon\hat{K}\right) \pm \sqrt{\cos^2\hat{\theta}\cos^2\gamma\left(1+\epsilon\hat{K}\right)^2 - \left(1-\epsilon^2\hat{K}\right)\left(1-\hat{K}\right)}\right]. \tag{126}$$

In analogy to the K observable for the $B_d^0 \to \pi^-\pi^+$, $B_s^0 \to K^-K^+$ system, $\hat{K}$ is not a clean observable because it depends on $|\hat{\mathcal{C}}/\hat{\mathcal{C}}'|$. This ratio is sensitive to both factorizable and non-factorizable U-spin-breaking corrections.

Fig. 11 shows the relation between $\hat{d}$ and $\hat{\theta}$ with 1σ error bands for the current data. As the penguin-annihilation topologies are loop suppressed while the exchange contributions arise at the tree level, we obtain the following naive – but plausible – upper bound:

$$\hat{d} \lesssim \frac{1}{R_b} \approx 2.56 \pm 0.20, \tag{127}$$

which we have included as a constraint in Fig. 11. Measurements of the CP-violating observables of these channels will allow a clean determination of the hadronic parameters $\hat{d}$ and $\hat{\theta}$. In order to explore their expected ranges, we employ the correlation between $\hat{d}$ and $\hat{\theta}$ in Fig. 11 to calculate a correlation between the direct and mixing-induced CP asymmetries. To this end, we use $\gamma = (70\pm7)^\circ$, $\phi_d = (43.2\pm1.8)^\circ$ and $\phi_s = -(0.68\pm2.2)^\circ$ as determined from experiment. We obtain a surprisingly constrained situation, as shown in Fig. 12. The general relation between the CP asymmetries in Eq. (15) implies

$$[\mathcal{A}_{\rm CP}^{\rm dir}(B_s \to \pi^-\pi^+)]^2 + [\mathcal{A}_{\rm CP}^{\rm mix}(B_s \to \pi^-\pi^+)]^2 = 1 - [\mathcal{A}_{\Delta\Gamma}(B_s \to \pi^-\pi^+)]^2 \leq 1. \tag{128}$$

Interestingly, we find CP asymmetries of the $B_d^0 \to K^-K^+$ channel that are scattered pretty close to this relation.

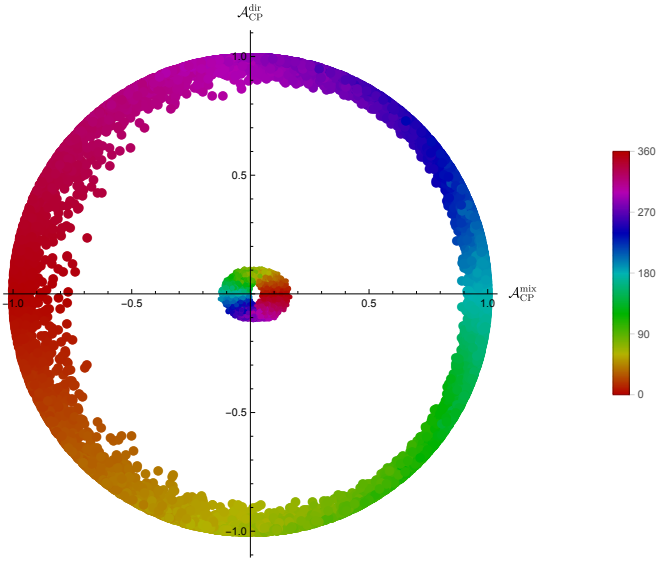

Figure 12: Correlation between the predicted direct and mixing-induced CP asymmetries of $B_d^0 \to K^-K^+$ (outer region) and for $B_s^0 \to \pi^-\pi^+$ (inner region). The colour coding indicates the value of the strong phase $\hat{\theta}$ [deg].

Future measurements of CP violation in $B_d^0 \to K^-K^+$ and $B_s^0 \to \pi^-\pi^+$ can unambiguously determine the parameters $\hat{d}$ and $\hat{\theta}$ and their U-spin counterparts $\hat{d}'$ and $\hat{\theta}'$, without making use of U-spin assumptions or relying on the $\hat{K}$ observable. Using then these parameters in the expression for $\hat{K}$ in Eq. (123), we may extract the amplitude ratio $|\hat{\mathcal{C}}/\hat{\mathcal{C}}'|$. These studies will allow us to explore U-spin-breaking effects in exchange and penguin annihilation topologies and will offer valuable further insights into the dynamics of these contributions.

6.2 Indirect Determinations of x

The direct determination of the exchange and penguin-annihilation topologies from the decays $B_d^0 \to K^-K^+$ and $B_s^0 \to \pi^-\pi^+$ can be complemented with indirect information from the ratios of branching ratios $\Xi_i^{(\prime)}$ listed in Table 6:

$$\Xi(B_x \to XX', B_y \to YY') \equiv \left[\frac{m_{B_x}}{m_{B_y}} \frac{\Phi(m_Y/m_{B_y}, m_{Y'}/m_{B_y})}{\Phi(m_X/m_{B_x}, m_{X'}/m_{B_x})} \frac{\tau_{B_y}}{\tau_{B_x}}\right] \frac{\mathcal{B}(B_x \to XX')}{\mathcal{B}(B_y \to YY')}\,, \quad (129)$$

where Φ is the phase-space function in Eq. (25). Although the theoretical interpretation of these quantities is affected by U-spin-breaking corrections, we have plenty of data available, allowing us to constrain the parameter x. For this analysis, also the penguin parameters (d, θ) and their counterparts are required. Future data will allow us to probe x' through the Ξ_i' ratios. In Subsections 6.4 and 6.5, we will discuss the optimal strategy for a future determination of Ξ_x and Ξ_P, respectively.

	Definition	Input	Factor	
Ξ_1	$\Xi(B_d \to K^-K^+, B_d \to \pi^-\pi^+)$	$(d,\theta),\hat{d}$	$\lvert\frac{x}{1+x}\rvert$ vs $\hat{\theta}$	Figs. 13(a) and 14
Ξ_2	$\Xi(B_d \to \pi^-\pi^+, B_s \to K^-\pi^+)$	$(d,\theta),(\tilde{d},\tilde{\theta})$	$\lvert 1+x\rvert$	Fig. 14
Ξ_3	$\Xi(B_d \to K^-K^+, B_s \to K^-\pi^+)$	$(\tilde{d},\tilde{\theta}),\hat{d}$	$\lvert x\rvert$ vs $\hat{\theta}$	Figs. 13(b) and 14
Ξ'_1	$\Xi(B_s \to \pi^-\pi^+, B_s \to K^-K^+)$	- (*)	$\lvert\frac{r'_{PA}}{1+r'_{PA}}\rvert$	Figs. 15 and 16
Ξ'_2	$\Xi(B_s \to K^-K^+, B_d \to \pi^-K^+)$	- (*)	$\lvert 1+r'_{PA}\rvert$	Fig. 16
Ξ'_3	$\Xi(B_s \to \pi^-\pi^+, B_d \to \pi^-K^+)$	- (*)	$\lvert r'_{PA}\rvert$	Fig. 16

Table 6: Definitions of the ratios of $B \to hh$ branching ratios and the parameters that they constrain in the current situation. At the moment, the Ξ'_i ratios constrain r'_{PA}. In the future, when independent information on the penguin parameters will be available, these ratios can be used to determine x' as well, as indicated by the asterix.

Let us first consider the ratio

$$\Xi_1 = \left|\frac{\hat{\mathcal{C}}}{\mathcal{C}}\right|^2 \left[\frac{1-2\hat{d}\cos\hat{\theta}\cos\gamma+\hat{d}^2}{1-2d\cos\theta\cos\gamma+d^2}\right] \ . \tag{130}$$

Defining

$$\eta \equiv \left|\frac{\hat{E}+\hat{P}A^{(ut)}}{E+PA^{(ut)}}\right| \sim \left(\frac{f_K}{f_\pi}\right)^2 = 1.423 \pm 0.006 \ , \tag{131}$$

where we have used the decay constants to estimate the non-factorizable topologies [12], yields

$$\left|\frac{\hat{\mathcal{C}}}{\mathcal{C}}\right|^2 = \left|\frac{x}{1+x}\right|^2 \eta^2 \ . \tag{132}$$

Consequently, we write

$$\Xi_1 = \left|\frac{x}{1+x}\right|^2 \eta^2 \left[\frac{1-2\hat{d}\cos\hat{\theta}\cos\gamma+\hat{d}^2}{1-2d\cos\theta\cos\gamma+d^2}\right] \stackrel{\rm exp}{=} 0.016 \pm 0.003 \ , \tag{133}$$

where the numerical value refers to the experimental branching ratios in Table 2. Using d and θ as determined from the CP-violating observables of the $B^0_d \to \pi^-\pi^+$ channel and $\hat{d}$ as a function of $\hat{\theta}$, as described by Eq. (126) and shown in Fig. 11, we may determine $|x|/|1+x|$ as a function of $\hat{\theta}$. The corresponding constraints are shown in Fig. 13(a).

Let us next consider the ratio

$$\Xi_2 = \left|\frac{\mathcal{C}}{\tilde{\mathcal{C}}}\right|^2 \left\langle\left|\frac{1-de^{i\theta}e^{-i\gamma}}{1-\tilde{d}e^{i\tilde{\theta}}e^{-i\gamma}}\right|^2\right\rangle \ , \tag{134}$$

where

$$\left|\frac{\mathcal{C}}{\tilde{\mathcal{C}}}\right|^2 = |1+x|^2\rho^2 \tag{135}$$

with

$$\rho \equiv \left|\frac{T+P^{(ut)}}{\tilde{T}+\tilde{P}^{(ut)}}\right| \ . \tag{136}$$

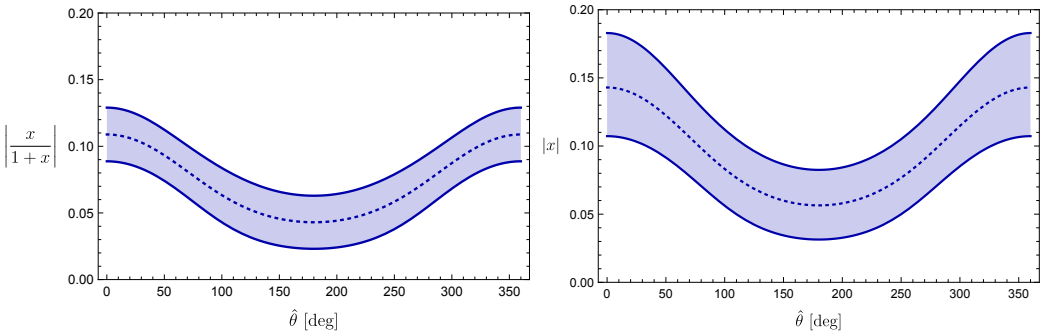

(a) (b)

Figure 13: Constraints on (a) the ratio $|x|/|1+x|$ and (b) $|x|$ as a function of $\hat{\theta}$.

We estimate ρ by considering the ratio of the relevant colour-allowed tree amplitudes in factorization, i.e.

$$\rho \sim \left|\frac{T}{\tilde{T}}\right|_{\text{fact}} = \left[\frac{m_{B_d}^2 - m_\pi^2}{m_{B_s}^2 - m_K^2}\right]\left[\frac{F_0^{B_d\pi}(m_\pi^2)}{F_0^{B_sK}(m_\pi^2)}\right] = 0.85^{+0.07}_{-0.13} \ , \tag{137}$$

where we have again used $F_0^{B_sK}(0)/F_0^{B_d\pi}(0) = 1.15^{+0.17}_{-0.09}$ from LCSR calculations [22], which agrees with the analysis of Ref. [23]. Finally, we use the unprimed equivalent of Eq. (70), which leads to

$$\frac{1 - de^{i\theta}e^{-i\gamma}}{1 - \tilde{d}e^{i\tilde{\theta}}e^{-i\gamma}} = \frac{1 - \tilde{d}e^{i\tilde{\theta}}e^{-i\gamma}/\zeta}{1 - \tilde{d}e^{i\tilde{\theta}}e^{-i\gamma}} \approx 1 \tag{138}$$

for $\zeta \sim 1$.

From the current experimental data, we extract

$$\Xi_2 \approx |1+x|^2\rho^2 \stackrel{\text{exp}}{=} 0.90 \pm 0.10 \ , \tag{139}$$

which yields

$$|1+x| = 1.12^{+0.18}_{-0.11} \ . \tag{140}$$

The large uncertainty comes from the form factors, and actually makes this ratio less powerful. However, we can nevertheless use it to constrain the phase of x introduced in Eq. (48), as shown in Fig. 14.

Finally, we consider

$$\Xi_3 = \left|\frac{\hat{\mathcal{C}}}{\tilde{\mathcal{C}}}\right|^2 \left[\frac{1 - 2\hat{d}\cos\hat{\theta}\cos\gamma + \hat{d}^2}{1 - 2\tilde{d}\cos\tilde{\theta}\cos\gamma + \tilde{d}^2}\right] \tag{141}$$

with

$$\left|\frac{\hat{\mathcal{C}}}{\tilde{\mathcal{C}}}\right|^2 = \eta^2\rho^2|x|^2 \ . \tag{142}$$

Using the branching ratios in Table 2 gives

$$\Xi_3 \simeq \eta^2\rho^2|x|^2 \left[\frac{1 - 2\hat{d}\cos\hat{\theta}\cos\gamma + \hat{d}^2}{1 - 2\tilde{d}\cos\tilde{\theta}\cos\gamma + \tilde{d}^2}\right] \stackrel{\text{exp}}{=} 0.014 \pm 0.003 \ . \tag{143}$$

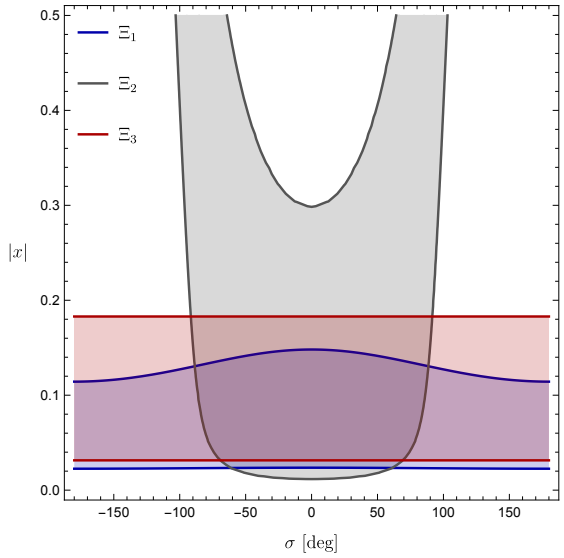

Figure 14: Constraints on $|x|$ and the phase σ from Ξ_2. The horizontal lines are conservative bounds from Ξ_1 and Ξ_3, as explained in the text.

If we use $\tilde{d}$ and $\tilde{\theta}$ as determined in Subsection 5.3 and $\hat{d}$ from Eq. (126), we may calculate $|x|$ as a function of $\hat{\theta}$, as shown in Fig. 13(b). The bound on $|x|$ varies between 0.03 and 0.18, which is consistent with the determination shown in Fig. 13(a).

For obtaining a complete picture, we have added the constraints from Fig. 13 to Fig. 14. Lacking information about the phase $\hat{\theta}$, we have conservatively used the upper bound at $\hat{\theta} = 0°$ and the lower bound at $\hat{\theta} = 180°$ from Fig. 13, since the values of $|x|/|1+x|$ and $|x|$ are largest and smallest there, respectively.

Unfortunately, the phase σ is only poorly constrained. More interesting is the current constraint of $|x| < 0.2$ from Ξ_3. Combining all constraints gives

$$|1+x| = 1.1 \pm 0.1 \ . \tag{144}$$

We further discuss this parameter and its implications for the ratio Ξ_x in Subsection 6.4.

6.3 Indirect Information on r'_{PA}

At the moment, only the ratios Ξ'_i defined in Table 6 can be used to study r'_{PA}. We may simplify the following discussion by assuming that the quantity ϵ, which enters the Ξ'_i, is small in comparison with the penguin parameters.

Let us first consider

$$\Xi'_1 = \left|\frac{\hat{\mathcal{C}}'}{\mathcal{C}'}\right|^2 \left[\frac{\epsilon^2 + 2\epsilon\hat{d}'\cos\hat{\theta}'\cos\gamma + \hat{d}'^2}{\epsilon^2 + 2\epsilon d'\cos\theta'\cos\gamma + d'^2}\right] \approx \left|\frac{\hat{\mathcal{C}}'}{\mathcal{C}'}\right|^2 \left(\frac{\hat{d}'}{d'}\right)^2 \ , \tag{145}$$

where we have ignored terms of $\mathcal{O}(\epsilon)$. We parametrize the penguin-annihilation amplitudes through

$$\eta' \equiv \left|\frac{\hat{PA}^{(ct)\prime}}{PA^{(ct)\prime}}\right| \sim \left(\frac{f_\pi}{f_K}\right)^2 = 0.703 \pm 0.003 \ , \tag{146}$$

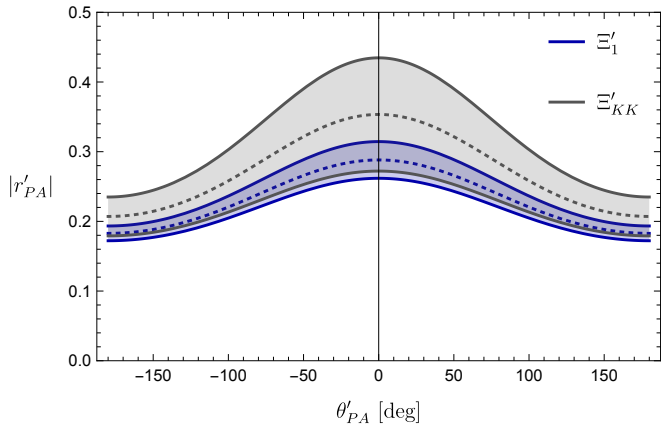

Figure 15: Constraints on $|r'_{PA}|$ and the phase θ'_{PA} from $B_s^0 \to \pi^-\pi^+$, $B_s^0 \to K^-K^+$ and $B_s^0 \to \pi^-\pi^+$, $B_s^0 \to K^0\overline{K}^0$ with 1σ error bands.

where we have used an approximation similar to Eq. (131). Note that in this approximation $\eta' = 1/\eta$. We find

$$\Xi'_1 = \left|\frac{r'_{\rm PA}}{1+r'_{\rm PA}}\right|^2 \eta'^2 \stackrel{\rm exp}{=} 0.025 \pm 0.004, \tag{147}$$

which leads to a contour in the complex plane of

$$r'_{PA} \equiv |r'_{PA}| e^{i\theta'_{PA}} \ , \tag{148}$$

as shown in Fig. 15.

In addition, we can consider

$$\Xi'_{KK} = \Xi(B_s^0 \to \pi^-\pi^+, B_s^0 \to K^0\overline{K}^0) \sim \left|\frac{\hat{\mathcal{C}}'}{\mathcal{C}'_{KK}}\right|^2 \hat{d}'^2 \ , \tag{149}$$

where we have neglected the penguin contribution d'_{KK} from $B_s^0 \to K^0\overline{K}^0$ since it is suppressed by ϵ. Using the experimental branching ratio for $B_s^0 \to K^0\overline{K}^0$ given in Eq. (93) yields

$$\Xi'_{KK} \sim \left(\frac{f_\pi}{f_K}\right)^4 \left|\frac{r'_{\rm PA}}{1+r'_{\rm PA}}\right|^2 \stackrel{\rm exp}{=} 0.034 \pm 0.011 \ . \tag{150}$$

The constraint from this ratio is in perfect agreement with that obtained from Ξ'_1, as illustrated in Fig. 15. This shows once again the importance of $B_s^0 \to K^0\overline{K}^0$ and the potential of future measurements of this decay. Next, we consider the ratio

$$\Xi'_2 = \left|\frac{\mathcal{C}'}{\tilde{\mathcal{C}}'}\right|^2 \left\langle \left|\frac{1+d'/\epsilon e^{i\theta'}e^{-i\gamma}}{1+\tilde{d}'/\epsilon e^{i\tilde{\theta}'}e^{-i\gamma}}\right|^2 \right\rangle \tag{151}$$

with

$$\left|\frac{\mathcal{C}'}{\tilde{\mathcal{C}}'}\right|^2 = |1+x'|^2\rho'^2 \ , \tag{152}$$

where ρ' is the equivalent of ρ defined in Eq. (136). Making the same approximations for ρ' as for ρ, we find

$$\rho' = 1/\rho = 1.18^{+0.17}_{-0.09}. \tag{153}$$

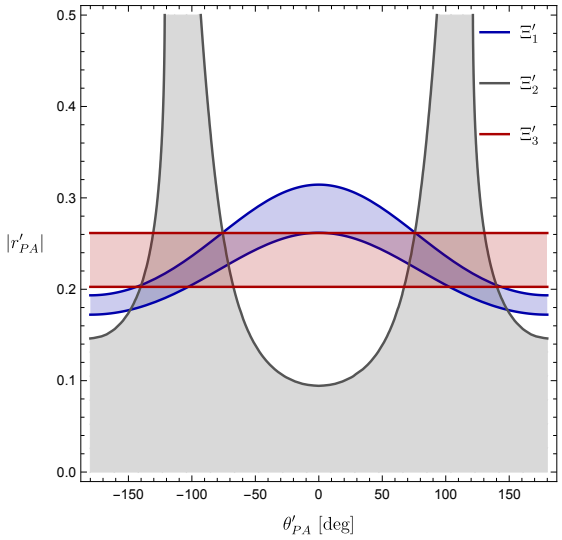

Figure 16: Bounds on $|r'_{PA}|$ and the phase θ'_{PA} using Ξ'_1, Ξ'_2 and Ξ'_3.

Neglecting again $\mathcal{O}(\epsilon)$ terms gives

$$\frac{1+\frac{1}{\epsilon}d'e^{i\theta'}e^{-i\gamma}}{1+\frac{1}{\epsilon}\tilde{d}'e^{i\tilde{\theta}'}e^{-i\gamma}} = \frac{\epsilon+\tilde{d}'e^{i\tilde{\theta}'}e^{-i\gamma}(\zeta')^{-1}}{\epsilon+\tilde{d}'e^{i\tilde{\theta}'}e^{-i\gamma}} \approx \frac{1+r'_{PA}}{1+x'} \ . \tag{154}$$

Using the experimental branching ratios in Table 2, we obtain

$$\Xi'_2 \approx \rho'^2|1+r'_{PA}|^2 \stackrel{\text{exp}}{=} 1.41 \pm 0.10 \ , \tag{155}$$

which leads to

$$|1+r'_{PA}| = 1.01^{+0.09}_{-0.15} \ . \tag{156}$$

We write $r'_{PA} \equiv |r'_{PA}|e^{\theta'_{PA}}$ and give the constraints from Ξ'_2 in Fig. 16. In analogy to Ξ_2, we observe that the constraint for $|1+r'_{PA}|$ suffers from large uncertainties due to the required form-factor information. Consequently, the ratios Ξ_2 and Ξ'_2 are at the moment only useful to constrain the phases of x and r'_{PA}, respectively. Information on their actual magnitude is more stringently constrained by the ratios $\Xi_1^{(\prime)}$ and $\Xi_3^{(\prime)}$.

Finally, we have the ratio

$$\Xi'_3 = \left|\frac{\hat{\mathcal{C}}'}{\tilde{\mathcal{C}}'}\right|^2 \left[\frac{\epsilon^2+2\epsilon\hat{d}'\cos\hat{\theta}'\cos\gamma+\hat{d}'^2}{\epsilon^2+2\epsilon\tilde{d}'\cos\tilde{\theta}'\cos\gamma+\tilde{d}'^2}\right] \approx \left|\frac{\hat{\mathcal{C}}'}{\tilde{\mathcal{C}}'}\right|^2 \left(\frac{\hat{d}'}{\tilde{d}'}\right)^2 \ , \tag{157}$$

where we neglect once again terms of $\mathcal{O}(\epsilon)$. Defining

$$\tilde{\rho}' \equiv \left|\frac{P^{(ct)\prime}}{\tilde{P}^{(ct)\prime}}\right| , \tag{158}$$

and making the approximation $\tilde{\rho}' \approx \rho'$ gives

$$\Xi'_3 \approx \tilde{\rho}'^2\eta'^2|r'_{PA}|^2 \stackrel{\text{exp}}{=} 0.035 \pm 0.004 \ , \tag{159}$$

yielding

$$|r'_{PA}| = 0.23^{+0.02}_{-0.04} \ . \tag{160}$$

In Fig. 16, we show the contour fixed through this ratio in the complex plane.

We have also added the constraint from Ξ'_1 to Fig. 16, and conclude that the current data favour slightly the regions around $\theta'_{PA} = \pm 100°$, while the constraint for $|r'_{PA}|$ is governed by the Ξ'_3 ratio.

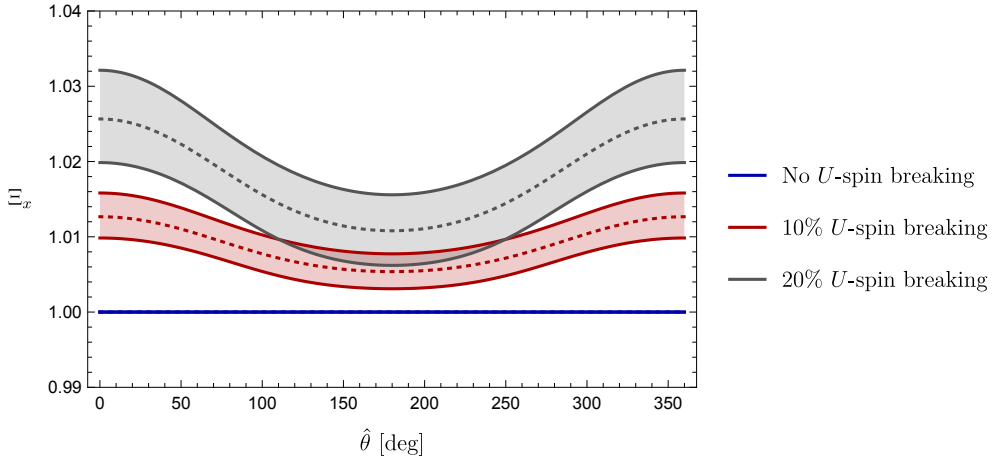

Figure 17: The ratio Ξ_x as a function of $\hat{\theta}$ for different U-spin-breaking effects.

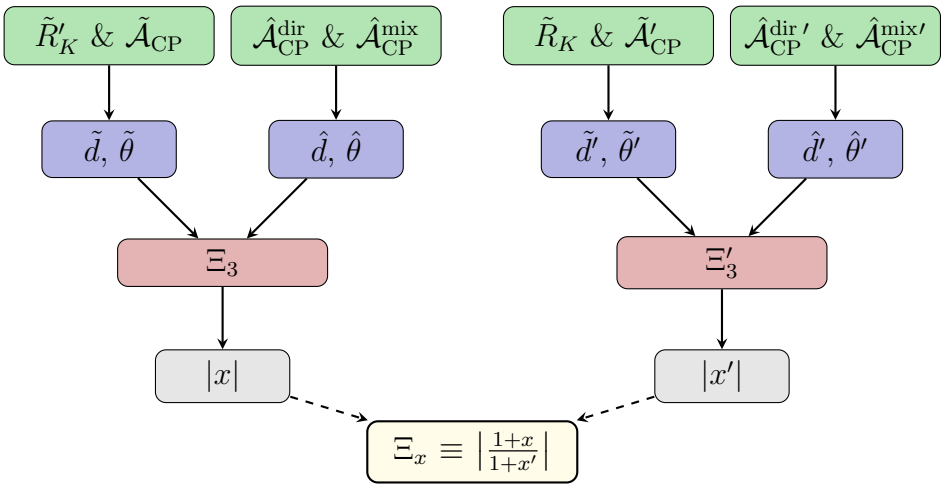

Figure 18: Strategy to determine Ξ_x. The $\tilde{\mathcal{A}}'_{\rm CP}$, $\tilde{\mathcal{A}}_{\rm CP}$ denote the direct CP asymmetries in $B^0_d \to \pi^- K^+$ and $B^0_s \to K^- \pi^+$, respectively, and $\hat{\mathcal{A}}^{\rm dir}_{\rm CP}$, $\hat{\mathcal{A}}^{\rm mix}_{\rm CP}$ and $\hat{\mathcal{A}}^{\rm dir\,\prime}_{\rm CP}$,$\hat{\mathcal{A}}^{\rm mix\prime}_{\rm CP}$ are the CP asymmetries of $B^0_d \to K^- K^+$ and $B^0_s \to \pi^- \pi^+$, respectively.

6.4 Determination of Ξ_x

The previous studies allow us to determine Ξ_x defined in Eq. (63) with the help of current data. The ratios Ξ_1, Ξ_2 and Ξ_3 provide information on $|x|$ and its phase σ. Independent information on x' is currently not available, but can be obtained from future measurements of CP violation in $B^0_s \to \pi^- \pi^+$. We consider

$$\Xi_x = \left|\frac{1+x}{1+x'}\right| = 1 + x\xi_x + \mathcal{O}(x^2), \tag{161}$$

where ξ_x is an $SU(3)$-breaking parameter defined through $x' = x(1-\xi_x)$. An important advantage of our strategy is that the exchange and penguin-annihilation topologies only contribute through the ratio Ξ_x. Since x is a small quantity, Ξ_x is very robust with respect to U-spin-breaking effects. This feature is illustrated in Fig. 17, which shows the ratio Ξ_x as a function of $\hat{\theta}$ for different U-spin-breaking effects. Allowing for 20% U-spin-breaking

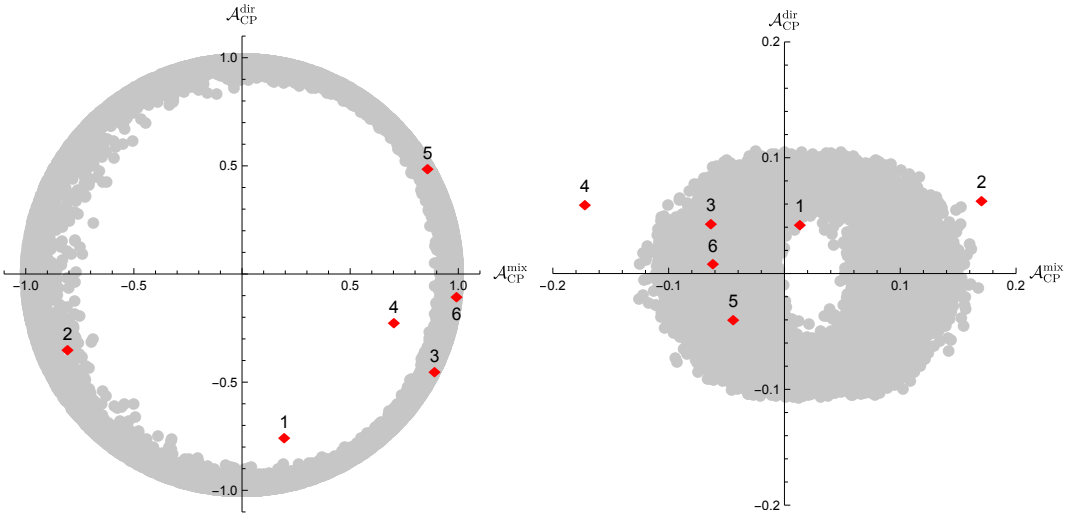

(a) $B_d^0 \to K^-K^+$ (b) $B_s^0 \to \pi^-\pi^+$

Figure 19: Correlation between the direct and mixing-induced CP asymmetries of $B_d^0 \to K^-K^+$ and of $B_s^0 \to \pi^-\pi^+$ as in Fig. 12, with the different scenarios indicated by diamonds.

only gives an uncertainty of $\mathcal{O}(4\%)$ for Ξ_x. However, especially around $\hat{\theta} = 180°$, which is actually the expected region, the effect can be much smaller. Future determinations of the CP asymmetries in the $B_d^0 \to K^-K^+$, $B_s^0 \to \pi^-\pi^+$ system can pinpoint these effects further, as illustrated in Fig. 18. The $B_d^0 \to K^-K^+$, $B_s^0 \to \pi^-\pi^+$ CP asymmetries allow a determination of $\hat{d}^{(\prime)}$, $\hat{\theta}^{(\prime)}$, while the semileptonic ratios $\tilde{R}'_K$ and $\tilde{R}_K$ would allow an independent determination of $\tilde{d}'$, $\tilde{\theta}'$. Finally, $|x^{(\prime)}|$ can be determined using $\Xi_3^{(\prime)}$ and $\tilde{d}^{(\prime)}$, $\tilde{\theta}^{(\prime)}$. This would give a clean determination of both $|x|$ and $|x'|$ independently, allowing a direct determination of Ξ_x, without any U-spin assumptions.

We further illustrate the use of the $B_d^0 \to K^-K^+$, $B_s^0 \to \pi^-\pi^+$ CP asymmetries by discussing six possible future scenarios, given in Table 7. The specific scenarios are also indicated in Fig. 19, and we assume the same relative uncertainties as those of the current measurements of the $B_d^0 \to \pi^-\pi^+$, $B_s^0 \to K^-K^+$ CP asymmetries.

For the different scenarios, $\hat{d}$ and $\hat{\theta}$ are extracted from the $B_d^0 \to K^-K^+$ CP asymmetries, using $\gamma = (70 \pm 1)°$ and $\phi_d = (43.2 \pm 0.6)°$ as before. This gives two solutions, where we discard the one which leads to anomalously large U-spin-breaking effects. The results are collected in Table 7. For scenarios 1, 2 and 4, the analytic expression is used to obtain the uncertainty. However, for scenarios 3, 5 and 6, the 1σ ranges are obtained from a χ^2 fit to take into account the correlated erros (see Fig. 20). The different values that were obtained are also indicated in Fig. 11. In addition, the parameters $\hat{d}'$ and $\hat{\theta}'$ are determined from the CP asymmetries of the $B_s^0 \to \pi^-\pi^+$ channel, using the central value of the current PDG average $\phi_s = -(0.68 \pm 0.5)°$ with an error expected for the era of Belle II and the LHCb upgrade.

Some of the obtained parameters $(\hat{d}, \hat{\theta})$ in Table 7 have large uncertainties. In particular scenarios 5 and 6 fall into this category as the mixing-induced CP asymmetries are close to 1. Since the CP asymmetries in $B_d^0 \to K^-K^+$ saturate the relation in Eq. (128), the corresponding direct CP asymmetries are constrained to values around 0. This feature reduces significantly the sensitivity to $(\hat{d}, \hat{\theta})$. The various scenarios are also illustrated in Fig. 20, which shows the contours in the $\hat{d}$–$\hat{\theta}$ plane following from the

No.	$\hat{\mathcal{A}}_{\rm CP}^{\rm dir}$ $\hat{\mathcal{A}}_{\rm CP}^{\rm dir\prime}$	$\hat{\mathcal{A}}_{\rm CP}^{\rm mix}$ $\hat{\mathcal{A}}_{\rm CP}^{\rm mix\prime}$	$\hat{d}$ $\hat{d}'$	$\hat{\theta}$ [deg] $\hat{\theta}'$ [deg]	$\lvert\hat{\mathcal{C}}/\hat{\mathcal{C}}'\rvert$
1	-0.75 ± 0.12 0.043 ± 0.034	0.20 ± 0.02 0.014 ± 0.006	2.0 ± 0.4 2.0 ± 1.2	60.0 ± 7.6 60.0 ± 22.6	1.44 ± 0.87
2	-0.35 ± 0.06 0.064 ± 0.050	-0.81 ± 0.07 0.17 ± 0.07	0.50 ± 0.07 0.50 ± 0.20	20.0 ± 3.6 20.0 ± 16.3	0.80 ± 0.30
3	-0.45 ± 0.07 0.044 ± 0.034	0.89 ± 0.08 -0.063 ± 0.027	$[0.9, 3.1]$ $[1.0, 2.8]$	$[121, 149]$ $[114, 170]$	$[0.41, 2.85]$
4	-0.22 ± 0.04 0.060 ± 0.047	0.70 ± 0.06 -0.17 ± 0.07	0.60 ± 0.09 0.60 ± 0.25	160.0 ± 3.3 160.0 ± 16.9	0.66 ± 0.28
5	0.49 ± 0.08 -0.039 ± 0.031	0.86 ± 0.08 -0.044 ± 0.019	$[0.9, 3.1]$ $[1.3, 4.2]$	$[214, 244]$ $[194, 255]$	$[0.54, 4.33]$
6	-0.10 ± 0.02 0.0089 ± 0.0070	0.99 ± 0.09 -0.062 ± 0.027	$[1.0, 4.4]$ $[1.3, 4.3]$	$[163, 173]$ $[154, 178]$	$[0.39, 3.91]$

Table 7: Overview of the different scenarios for the CP-violating observables of the $B_d^0 \to K^-K^+$ and $B_s^0 \to \pi^-\pi^+$ decays.

direct (blue) and mixing-induced (red) CP asymmetries of the $B_d^0 \to K^-K^+$ channel, along with the 1σ contour from a χ^2 fit of these two observables.

We notice that the amplitude ratio $|\hat{\mathcal{C}}/\hat{\mathcal{C}}'|$ in Eq. (123) can unfortunately only be determined with limited precision in our scenarios. The results are summarized in Table 7, where the ranges correspond to the allowed regions of the penguin parameters.

Finally, implementing the strategy illustrated in Fig. 18, we can determine $|x|$ and $|x'|$. Based on the definition in Eq. (122), we expect the strong phases $\hat{\theta}^{(\prime)}$ to take values around 180°. Let us therefore consider scenario 6, where in addition $\hat{d}$ is close to the prediction from Eq. (126), and scenario 4, where $\hat{d}$ is closer to the value of d.

With the input from scenario 6 (S_6), we find

$$\left|\frac{x}{1+x}\right|_{S_6} = [0.024, 0.071], \qquad |x|_{S_6} = [0.031, 0.093], \tag{162}$$

where the range corresponds to the allowed region of $\hat{d}$ and $\hat{\theta}$. If we assume scenario 4 (S_4), we find

$$\left|\frac{x}{1+x}\right|_{S_4} = 0.087 \pm 0.009, \qquad |x|_{S_4} = 0.11 \pm 0.02, \tag{163}$$

which has remarkably small uncertainties. Most important, even though the uncertainty for the extracted value of $\hat{d}$ might be significant, the impact on the determination of $|x|$ is small.

Interestingly, we can now also determine $|x'|$ with the help of Ξ_3'. At the moment, we cannot determine $\tilde{d}'$ and $\tilde{\theta}'$ in an independent way. However, as discussed in Subsection 5.3 and illustrated in Fig. 18, measurements of the semileptonic decay rates will change this situation. To illustrate this future determination, we consider the results in Eq. (114), yielding

$$|x'|_{S_6} = [0.028, 0.092], \qquad |x'|_{S_4} = 0.20^{+0.08}_{-0.09}\ . \tag{164}$$

These results are in impressive agreement with the constraints for $|x|$ in Eq. (162), and suggest small U-spin-breaking effects.

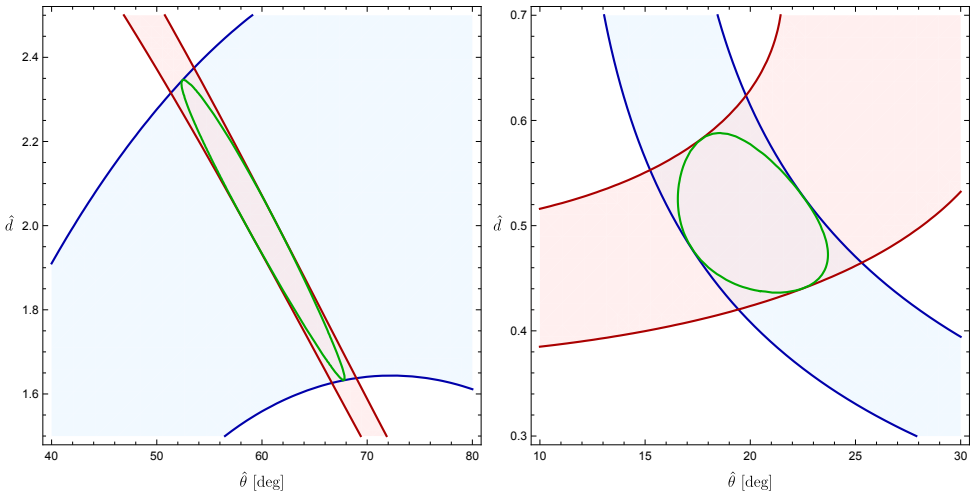

(a) Scenario 1

(b) Scenario 2

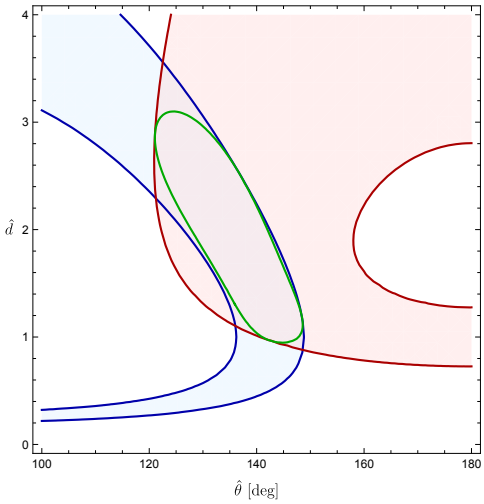

(c) Scenario 3

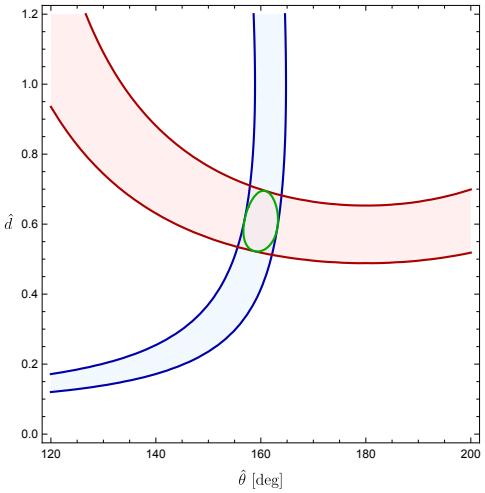

(d) Scenario 4

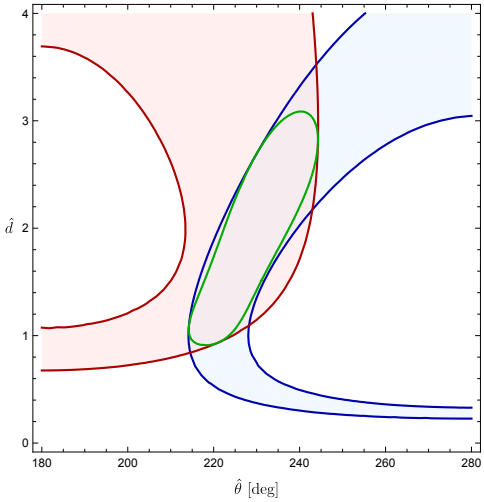

(e) Scenario 5

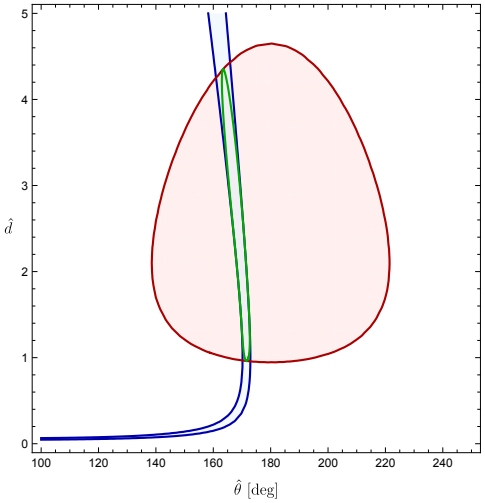

(f) Scenario 6

Figure 20: Determination of $\hat{d}$ and $\hat{\theta}$ from the CP-violating observables of $B_d^0 \to K^- K^+$. The blue and red contours follow from the direct and mixing-induced CP asymmetries, respectively. The 1σ contours resulting from a χ^2 fit are shown in green.

6.5 Determination of Ξ_P

It is instructive to write the ratio Ξ_P introduced in Eq. (63) as

$$\Xi_P = \frac{1+r_P}{1+r'_P} = 1 + r_P\xi_r + \mathcal{O}(r_P^2) \ , \tag{165}$$

where ξ_r is an U-spin-breaking parameter defined through

$$r'_P = r_P(1-\xi_r) \ . \tag{166}$$

As in Eq. (85), we may write r_P as a function of (d,θ) and ζ:

$$1 + r_P = \frac{1}{1-\zeta d e^{i\theta}\rho_P} \ , \tag{167}$$

where

$$\zeta \equiv |\zeta| e^{i\omega} \equiv \frac{1+x}{1+r_{PA}} \ ; \tag{168}$$

an analogous expression holds for $1 + r'_P$.

In our new strategy, we eventually determine d' and θ' from the data, while d and θ are fixed through the CP asymmetries of the $B_d^0 \to \pi^-\pi^+$ decay. Starting with $\Xi_P = 1$, as in the strict U-spin limit, we may include these effects in an iterative way.

The parameter ζ can be determined from our previous analysis. Taking $|1+x| = 1.1 \pm 0.1$ from Eq. (144) and $|1 + r'_{PA}| = 1.01^{+0.09}_{-0.15}$ as given in Eq. (156) yields

$$|\zeta| = 1.09^{+0.19}_{-0.14} \ . \tag{169}$$

Furthermore, ζ relates the penguin parameters in $B_d^0 \to \pi^-\pi^+$ and $B_d^0 \to \pi^- K^+$ through

$$\tilde{d} e^{i\tilde{\theta}} = \zeta d e^{i\theta} \ , \tag{170}$$

which is only affected by $SU(3)$-breaking effects at the spectator-quark level (see Eq. (69)).

We use now Eq. (170) to write

$$r_P = \frac{\rho_P \tilde{d} e^{i(\theta_P+\tilde{\theta})}}{1-\rho_P \tilde{d} e^{i(\theta_P+\tilde{\theta})}} \tag{171}$$

and

$$|1 + r_P| = \left| \frac{1}{1-\rho_P \tilde{d} e^{i(\theta_P+\tilde{\theta})}} \right| \ . \tag{172}$$

Applying the results for the penguin ratio ρ_P in Eq. (107), and using $(\tilde{d},\tilde{\theta})$ from Eq. (113), we find

$$|r_P| = 0.22 \pm 0.07 \tag{173}$$

and

$$|1 + r_P| = 0.79 \pm 0.07 \ , \tag{174}$$

where the uncertainties are dominated by those of ρ_P and θ_P. Using the numerical range in (173) and $\xi_r = 0.2$, i.e. assuming U-spin-breaking effects of 20%, the favourable structure of the Ξ_P ratio in Eq. (165) reduces these uncertainties to the 5% level.

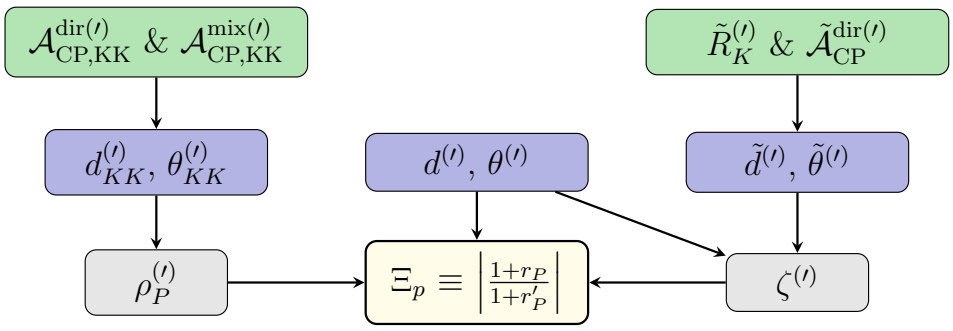

Figure 21: Strategy to determine Ξ_P. On the left-hand side, the strategy to determine ρ_P and ρ'_P is illustrated, while we show on the right hand side the strategy to improve ζ and ζ' using the semileptonic decay ratios.

Let us now explore how we may reduce the uncertainty of Ξ_P further through sophisticated analyses provided by future experimental data. We aim at an independent precise determination of r_P and its primed counterpart r'_P, whose uncertainties are dominated by (ρ_P, θ_P). In Subection 5.3, we discussed the achievable precision for the $B_d^0 \to K^0\overline{K}^0$ penguin parameters (d_{KK}, θ_{KK}), which – using the $SU(3)$ flavour symmetry – are equivalent to (ρ_P, θ_P). A determination of the CP asymmetries at the 0.05 level would lead to a determination of ρ_P with 0.03 uncertainty, giving in turn $r_P = 0.22 \pm 0.02$. The CP asymmetries for $B_s^0 \to K^0\overline{K}^0$, which have not yet been measured, would allow a determination of ρ'_P, thereby providing full information on U-spin-breaking effects in these penguin topologies. However, also improved information from the CP asymmetries in $B_d^0 \to K^0\overline{K}^0$ alone would already significantly reduce the uncertainty for Ξ_P, as determined from Eq. (165) and shown in Fig. 22. There the relation between Ξ_P and the uncertainty of the $B_d^0 \to K^0\overline{K}^0$ asymmetries is shown for different U-spin-breaking effects between r_P and r'_P defined by ξ_P. Consequently, the CP asymmetries in $B_d^0 \to K^0\overline{K}^0$ have the potential to reduce the uncertainty for Ξ_P significantly below the 4% level.

In addition, the input $(\tilde{d}, \tilde{\theta})$ and their primed analogues can be independently determined via the semileptonic ratios $\tilde{R}_K$ and $\tilde{R}'_K$ through the strategy illustrated in Fig. 21. Using Eq. (170), we may determine ζ and ζ', providing additional information into U-spin-breaking effects in exchange and penguin-annihilation topologies. In order to illustrate the future precision of this method, we consider (d, θ) and $(\tilde{d}, \tilde{\theta})$ for the upgrade scenario as given in Eqs. (42) and (114), respectively, which leads to an impressive precision of $|\zeta| = 0.93 \pm 0.05$ and $\omega = (4.0 \pm 1.3)^\circ$ as given in Eq. (116).

7 Prospects of the New Strategy

The precision for ϕ_s achievable with the new strategy depends on experimental and theoretical uncertainties. Experimentally, the precision with which the semileptonic ratios R_K and R_π can be determined dominate the uncertainty. In Subsection 4.2, we showed that a relative precision for R_K and R_π at the 5% level allows an impressive 0.5° uncertainty for $\Delta\phi_{KK}$. With the information obtained in the previous sections, we can now quantify the theoretical error for $\xi^a_{\rm NF}$. This uncertainty arises from U-spin-breaking effects in the ratios Ξ_x and Ξ_P. Fortunately, these ratios are very robust with respect to

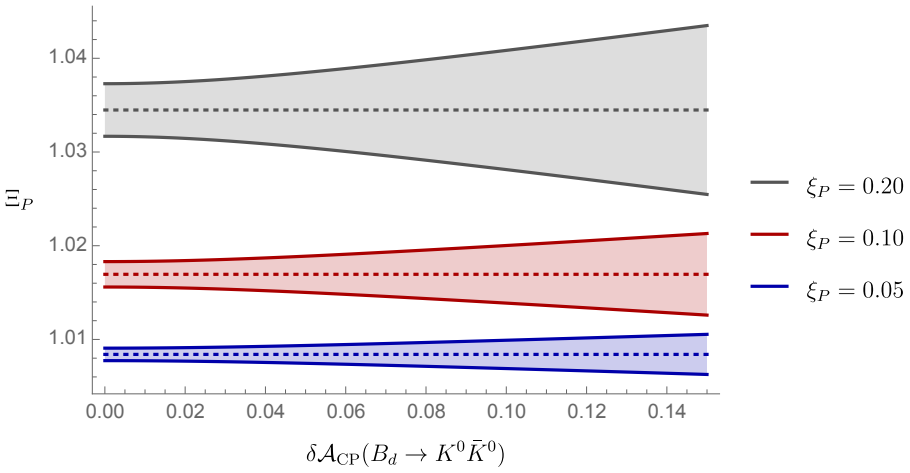

Figure 22: The ratio Ξ_P as a function of the precision of the CP asymmetries of the decay $B_d^0 \to K^0\overline{K}^0$ for different U-spin-breaking effects.

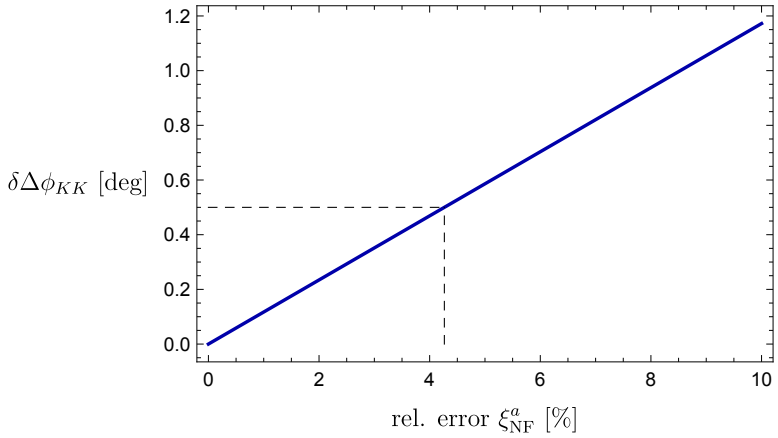

Figure 23: The uncertainty for $\Delta\phi_{KK}$ as a function of the relative error of $\xi^a_{\rm NF}$, assuming a perfect experimental situation.

these effects and can be obtained from experimental data.

For the current data, we obtain an uncertainty of 5% for Ξ_P, which can be further reduced with more precise data for the $B_d^0 \to K^0\overline{K}^0$ and $B_s^0 \to K^0\overline{K}^0$ CP asymmetries (see 5.1 and 6.5). In addition, we find an uncertainty of 4% for Ξ_x, which can also be further improved using the CP asymmetries of $B_d^0 \to \pi^-\pi^+$, $B_s^0 \to K^-K^+$ (see 6.4). The last source of uncertainty is related to the non-factorizable U-spin-breaking effects in the ratio of the colour-allowed tree topologies, which are theoretically well-behaved and give an error at the 1% level (see 4.2). Finally, adding up the individual errors in quadrature we find a precision of about 7% for $\xi^a_{\rm NF}$.

Fig. 23 gives the precision of $\Delta\phi_{KK}$ as a function of the relative error of $\xi^a_{\rm NF}$, assuming a perfect experimental situation. We observe that a 7% precision for $\xi^a_{\rm NF}$ gives a theoretical uncertainty at the 0.8° level for $\Delta\phi_{KK}$. Recalling that $\phi_s = \phi_s^{\rm eff} - \Delta\phi_{KK}$ and that a precision of 0.5° for $\phi_s^{\rm eff}$ can be reached in the upgrade era (Eq. (40)), we aim for a similar theoretical precision for $\Delta\phi_{KK}$, which is indicated by the dashed line in Fig. 23. Such a precision requires an $\mathcal{O}(4\%)$ determination of $\xi^a_{\rm NF}$, which is within reach in the upgrade era.

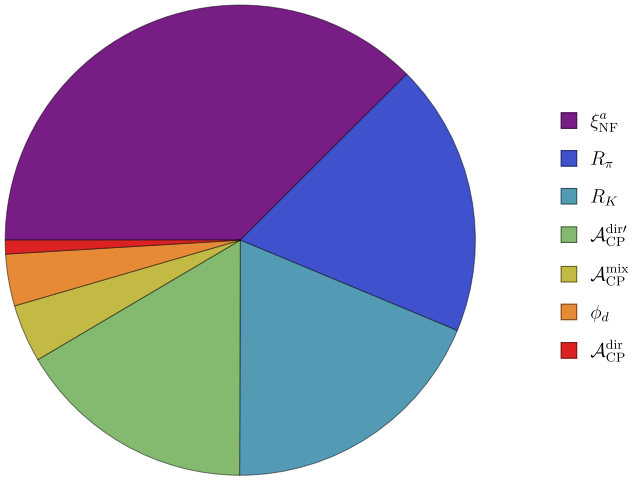

Figure 24: Error budget of the hadronic phase shift $\Delta\phi_{KK}$.

Combining now the experimental and theoretical uncertanties, assuming a relative precision of 5% for the relevant parameters R_π, R_K and $\xi^a_{\rm NF}$, results in an impressive uncertainty of 0.8° for $\Delta\phi_{KK}$. The error budget of $\Delta\phi_{KK}$ in this scenario is given in Fig. 24. This allows a determination of ϕ_s with a similar precision, which is a major improvement with respect to the current situation in Eq. (30).

Interestingly, our new method allows also the determination of the hadronic parameters d' and θ'. Assuming that R_K, R_π and $\xi^a_{\rm NF}$ can be determined with 5% uncertainty, we find

$$d' = 0.58 \pm 0.04 \;, \qquad \theta' = (151.4 \pm 3.5)^\circ \;, \tag{175}$$

showing a very impressive precision and providing valuable insights into the U-spin symmetry. In particular, we may now determine the U-spin-breaking parameters ξ and Δ in Eq. (35). For the upgrade scenario, ξ can be extracted with an uncertainty at the 0.07 level.

In addition, our method offers a test of QCD factorization in the $B^0_d \to \pi^-\pi^+$ and $B^0_s \to K^-K^+$ decays through the information for r_P and x. We have given the current experimental value for $|a_{\rm NF}|$ of the $B^0_d \to \pi^-\pi^+$ decay in Eq. (52):

$$|a_{\rm NF}| = |1 + r_P||1 + x||a^T_{\rm NF}| = 0.73 \pm 0.06 \;. \tag{176}$$

Using $|1 + x| = 1.1 \pm 0.1$ from Eq. (144) and $|1 + r_P| = 0.8 \pm 0.08$ from Eq. (174) yields

$$|a^T_{\rm NF}| = 0.82 \pm 0.13 \,, \tag{177}$$

which agrees with the QCD factorization calculation in Eq. (49) at the $1\,\sigma$ level.

A key element in the new strategy are the semileptonic differential rates and the corresponding R_π and R_K ratios. Since the $B^0_s \to K^-\ell^+\nu_\ell$ decay has not yet been measured, it is interesting to come back to the ratio K and the use of form-factor calculations as input. In this case, the ratios R_π and R_K are no longer required and we can write

$$r_K = r_\pi K, \tag{178}$$

where K is given in Eq. (24). The only difference with respect to our new strategy is that we have now to rely on theoretical input for the form-factor ratio $F^{B_sK}(m_K^2)/F^{B_d\pi}(m_\pi^2)$, replacing the ratio R_π/R_K which can be determined by means of experimental data. The non-factorizable U-spin-breaking effects are again described by the parameter $\xi^a_{\rm NF}$. The current determination of the form-factor ratio from LCSR, $F_0^{B_sK}(0)/F_0^{B_d\pi}(0) = 1.15^{+0.17}_{-0.09}$ [22], has still a significant uncertainty. However, dedicated efforts using lattice QCD and progress with LCSR analyses may lead to a sharper picture of $F^{B_sK}(m_K^2)/F^{B_d\pi}(m_\pi^2)$ in the future.

Let us consider the LHCb upgrade scenario, assuming $\xi^a_{\rm NF} = 1.00 \pm 0.05$. In Fig. 25, we show the precision of $\Delta\phi_{KK}$ as a function of the relative uncertainty of the form-factor ratio in comparison with relative precision of R_K/R_π using the new strategy. We observe that a good precision can be reached using the ratio K, provided it is possible to calculate form-factor ratio with a precision at the 5% level. However, it will be challenging to go beyond the precision of our new strategy, even if the experimental ratio R_K/R_π would only be known with 15% precision. Consequently, the new strategy, which does not rely on non-perturbative input for the form factors, is most powerful for extracting ϕ_s.

We may actually use our new strategy to determine $F^{B_sK}(m_K^2)/F^{B_d\pi}(m_\pi^2)$. Using the values of d, θ and d', θ', we may calculate K with the help of Eq. (24), which allows us to extract $|\mathcal{C}/\mathcal{C}'|$ from the ratio of the $B_s^0 \to K^-K^+$, $B_d^0 \to \pi^-\pi^+$ branching ratios, and write

$$\left|\frac{\mathcal{C}}{\mathcal{C}'}\right| \equiv \left|\frac{T}{T'}\right|_{\rm fact} \xi^a_{\rm NF} = \frac{f_\pi}{f_K}\left[\frac{m_{B_d}^2 - m_\pi^2}{m_{B_s}^2 - m_K^2}\right]\left[\frac{F_0^{B_d\pi}(m_\pi^2)}{F_0^{B_sK}(m_K^2)}\right]\xi^a_{\rm NF}\ . \tag{179}$$

For the current data, using Eqs. (79) and (113) and $\gamma = (70 \pm 7)^\circ$, we find

$$K = 57.2 \pm 14.4\ , \tag{180}$$

where we assumed $d' = \tilde{d}$ and $\theta' = \tilde{\theta}$, neglecting tiny exchange and penguin-annihilation topologies. Using $\xi^a_{\rm NF} = 1.00 \pm 0.07$ gives

$$\frac{F_0^{B_sK}(m_K^2)}{F_0^{B_d\pi}(m_\pi^2)} = 1.09 \pm 0.16, \tag{181}$$

which is in interesting agreement with the LCSR calculation. For the LHCb upgrade scenario, we expect that the precision for the ratio of form factors can be reduced to the 0.06 level.

8 Conclusions

The U-spin relation between the $B_d^0 \to \pi^-\pi^+$ and $B_s^0 \to K^-K^+$ decays has originally been proposed to extract the UT angle γ and the mixing phase ϕ_s [4–6]. The current experimental picture is already impressive, in agreement with the SM and uncertainties at the 7° level. The theoretical precision is limited by U-spin-breaking corrections, which do not allow us – unless there is significant progress to calculate them – to take full advantage of the data to be collected in the era of Belle II and the LHCb upgrade.

In view of this situation, we proposed a new strategy to fully exploit the physics potential of the non-leptonic $B_s^0 \to K^-K^+$ and $B_d^0 \to \pi^-\pi^+$ decays to extract ϕ_s [9]. The strategy utilizes the U-spin relation between these two decays for theoretically well

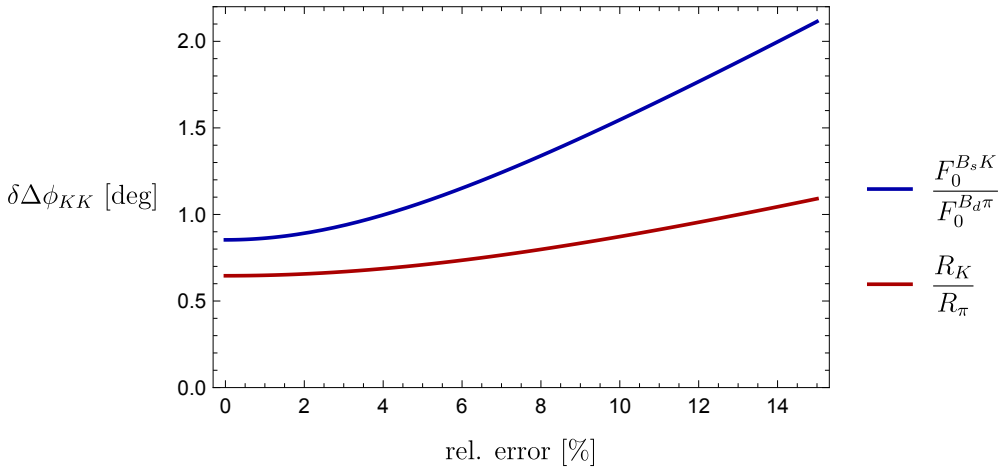

Figure 25: The dependence of the uncertainty of $\Delta\phi_{KK}$ on the relative error of the ratio of form factors using the ratio K, and R_K/R_π using the semileptonic decays.

behaved quantities, thereby resulting in a very robust situation with respect to U-spin-breaking effects. The new key elements are the differential rates of the semileptonic decays $B_d^0 \to \pi^-\ell^+\nu_\ell$ and $B_s^0 \to K^-\ell^+\nu_\ell$, which enter ratios with the $B_d^0 \to \pi^-\pi^+$ and $B_s^0 \to K^-K^+$ decay rates R_π and R_K, respectively. In fact, only the double ratio R_π/R_K enters our strategy, which is an advantage from the experimental point of view as uncertainties cancel. A theoretical advantage is that the form factors now enter only in a double ratio, which is equal to 1 with excellent precision. In our new strategy, non-factorizable U-spin-breaking corrections to the notoriously difficult to calculate penguin, exchange and penguin-annihilation topologies only contribute through the ratios Ξ_P and Ξ_x. As we have shown, these quantities are very robust with respect to U-spin-breaking effects. On the other hand, the original strategy is limited by leading non-factorizable U-spin-breaking effects that emerge from penguin topologies.

The CP-violating observables of $B_s^0 \to K^-K^+$ allow us to determine the "effective" B_s^0–$\overline{B}_s^0$ mixing phase $\phi_s^{\rm eff}$, which is a pure experimental quantity. In order to extract the mixing phase ϕ_s from $\phi_s^{\rm eff}$, we have to subtract the hadronic phase shift $\Delta\phi_{KK}$, which depends on non-perturbative quantities. In the upgrade era, $\phi_s^{\rm eff}$ can be measured with an uncertainty at the 0.5° level. Consequently, our goal is to match this very impressive experimental precision by theory, determining $\Delta\phi_{KK}$ with similar uncertainty.

Unfortunately, the $B_s^0 \to K^-\ell^+\nu_\ell$ decay, a key input for our new strategy, has not yet been measured. We strongly advocate analyses of this channel at Belle (II) and LHCb, preferably extracting R_K or the ratio R_π/R_K directly from the experimental data. In order to illustrate the strength of our new method, we use data for $B_d^0 \to \pi^-K^+$. This decay is related to $B_s^0 \to K^-K^+$ by a U-spin relation at the spectator quark level if the small contributions from exchange and penguin annihilation topologies are neglected. We find a precision for $\Delta\phi_{KK}$ of 0.6°, which shows impressively the power of our strategy. Moreover, we obtain excellent agreement with the picture of the U-spin symmetry, excluding anomalously large corrections.

The determination of $\Delta\phi_{KK}$ is affected by experimental and theoretical uncertainties. For a perfect theoretical situation, measurements of R_π and R_K with 5% precision are required to obtain a 0.5° precision for $\Delta\phi_{KK}$. The theoretical precision is limited by U-spin-breaking corrections to quantities which have very favourable structures. In order

to fully exploit the precision of our strategy, we need information both for the penguin ratio r_P and for the exchange and penguin-annihilation parameter x.

The penguin parameter r_P can be studied with the help of the pure penguin decays $B_d^0 \to K^0\overline{K}^0$ and $B_s^0 \to K^0\overline{K}^0$, which offer an interesting laboratory for the upgrade era. Since the current data for these modes are limited, we have also used the charged decays $B^+ \to K^+\overline{K}^0$ and $B^+ \to \pi^+K^0$ to constrain the size of r_P. In summary, using these decays, we find an uncertainty for the relevant ratio Ξ_p at the 5% level. We have presented a strategy to further reduce this uncertainty, as illustrated in Fig. 21.

Future measurements of the CP asymmetries of $B_d^0 \to K^-K^+$ and $B_s^0 \to \pi^-\pi^+$ allow us to determine the exchange and penguin-annihilation contributions with high precision. We have discussed the correlation between these CP asymmetries following from the current data, resulting in an interesting picture for the future data taking, and presented scenarios of future measurements and their use to pin down the exchange and penguin-annihilation contributions even further. For the current data, we use ratios of different $B \to hh$ $(h = \pi, K)$ decays and find a contribution of $x \sim 0.1$, which results in a theoretical uncertainty of $\mathcal{O}(4\%)$ for the exchange and penguin-annihilation ratio Ξ_x.

Combining the different sources of theoretical uncertainty, we find a theoretical precision of $\Delta\phi_{KK}$ at the 0.8° level. We have discussed different strategies to reduce this uncertainty further with future experimental data, and have illustrated them with various scenarios, showing that a future ultimate precision at the 0.5° level is within reach. Consequently, the new strategy has the potential to extract ϕ_s from CP violation in $B_s^0 \to K^-K^+$ with a theoretical precision matching experiment. The key question is whether the corresponding value will eventually show a discrepancy with respect to the clean SM prediction $\phi_s^{\rm SM}$ and determinations from other decays, in particular $B_s^0 \to J/\psi\phi$. Since $B_s^0 \to K^-K^+$ is dominated by QCD penguin topologies, which are sensitive to possible new heavy particles, we may actually find a surprise, fully exploiting the excellent experimental precision attainable at Belle II and the LHCb upgrade.

Acknowledgements

We would like to thank Kristof De Bruyn for very useful discussions and Vincenzo Vagnoni for correspondence. This work is supported by the Foundation for Fundamental Research on Matter (FOM) and by the Deutsche Forschungsgemeinschaft (DFG) within research unit FOR 1873 (QFET).

References

[1] A. J. Buras and J. Girrbach, Rept. Prog. Phys. **77** (2014) 086201 doi:10.1088/0034-4885/77/8/086201 [arXiv:1306.3775 [hep-ph]].

[2] T. Abe *et al.* [Belle-II Collaboration], arXiv:1011.0352 [physics.ins-det].

[3] R. Aaij *et al.* [LHCb Collaboration], Eur. Phys. J. C **73** (2013) 2373 doi:10.1140/epjc/s10052-013-2373-2 [arXiv:1208.3355 [hep-ex]].

[4] R. Fleischer, Phys. Lett. B **459** (1999) 306 doi:10.1016/S0370-2693(99)00640-1 [hep-ph/9903456].

[5] R. Fleischer, Eur. Phys. J. C **52** (2007) 267 doi:10.1140/epjc/s10052-007-0391-7 [arXiv:0705.1121 [hep-ph]].

[6] R. Fleischer and R. Knegjens, Eur. Phys. J. C **71** (2011) 1532 doi:10.1140/epjc/s10052-010-1532-y [arXiv:1011.1096 [hep-ph]].

[7] R. Aaij *et al.* [LHCb Collaboration], JHEP **1310** (2013) 183 doi:10.1007/JHEP10(2013)183 [arXiv:1308.1428 [hep-ex]].

[8] R. Aaij *et al.* [LHCb Collaboration], Phys. Lett. B **741** (2015) 1 doi:10.1016/j.physletb.2014.12.015 [arXiv:1408.4368 [hep-ex]].

[9] R. Fleischer, R. Jaarsma and K. K. Vos, arXiv:1608.00901 [hep-ph], to appear in Phys. Rev. D.

[10] M. Gronau, O. F. Hernandez, D. London and J. L. Rosner, Phys. Rev. D **50** (1994) 4529 doi:10.1103/PhysRevD.50.4529 [hep-ph/9404283].

[11] M. Gronau, O. F. Hernandez, D. London and J. L. Rosner, Phys. Rev. D **52** (1995) 6356 doi:10.1103/PhysRevD.52.6356 [hep-ph/9504326].

[12] C. Bobeth, M. Gorbahn and S. Vickers, Eur. Phys. J. C **75** (2015) 340 doi:10.1140/epjc/s10052-015-3535-1 [arXiv:1409.3252 [hep-ph]].

[13] L. Wolfenstein, Phys. Rev. Lett. **51** (1983) 1945.

[14] A. J. Buras, M. E. Lautenbacher and G. Ostermaier, Phys. Rev. D **50** (1994) 3433 doi:10.1103/PhysRevD.50.3433 [hep-ph/9403384].

[15] J. Charles *et al.*, Phys. Rev. D **91** (2015) no.7, 073007 doi:10.1103/PhysRevD.91.073007 [arXiv:1501.05013 [hep-ph]]; for updates, see `http://ckmfitter.in2p3.fr`.

[16] R. Fleischer, Phys. Rept. **370** (2002) 537 doi:10.1016/S0370-1573(02)00274-0 [hep-ph/0207108].

[17] M. Artuso, G. Borissov and A. Lenz, Rev. Mod. Phys. **88** (2016) no. 4, 045002 doi:10.1103/RevModPhys.88.045002 [arXiv:1511.09466 [hep-ph]].

[18] I. Dunietz, R. Fleischer and U. Nierste, Phys. Rev. D **63** (2001) 114015 doi:10.1103/PhysRevD.63.114015 [hep-ph/0012219].

[19] K. De Bruyn, R. Fleischer, R. Knegjens, P. Koppenburg, M. Merk and N. Tuning, Phys. Rev. D **86** (2012) 014027 doi:10.1103/PhysRevD.86.014027 [arXiv:1204.1735 [hep-ph]].

[20] Y. Amhis *et al.* [Heavy Flavor Averaging Group], arXiv:1412.7515 [hep-ex]. for updates, see `http://www.slac.stanford.edu/xorg/hfag/`.

[21] R. Aaij *et al.* [LHCb Collaboration], Phys. Lett. B **736** (2014) 446 doi:10.1016/j.physletb.2014.07.051 [arXiv:1406.7204 [hep-ex]].

[22] G. Duplancic and B. Melic, Phys. Rev. D **78** (2008) 054015 doi:10.1103/PhysRevD.78.054015 [arXiv:0805.4170 [hep-ph]].

[23] A. Khodjamirian, T. Mannel and M. Melcher, Phys. Rev. D **70** (2004) 094002 doi:10.1103/PhysRevD.70.094002 [hep-ph/0407226].

[24] J. L. Rosner, S. Stone and R. S. Van de Water, arXiv:1509.02220 [hep-ph].

[25] M. Gronau and D. Wyler, Phys. Lett. B **265** (1991) 172. doi:10.1016/0370-2693(91)90034-N

[26] D. Atwood, I. Dunietz and A. Soni, Phys. Rev. Lett. **78** (1997) 3257 doi:10.1103/PhysRevLett.78.3257 [hep-ph/9612433]; Phys. Rev. D **63** (2001) 036005 doi:10.1103/PhysRevD.63.036005 [hep-ph/0008090].

[27] R. Fleischer and S. Ricciardi, proceedings of the 6th International Workshop on the CKM Unitarity Triangle (CKM 2010) [arXiv:1104.4029 [hep-ph]].

[28] J. Charles *et al.* [CKMfitter Group Collaboration], Eur. Phys. J. C **41** (2005) 1 doi:10.1140/epjc/s2005-02169-1 [hep-ph/0406184], updated results and plots available at: `http://ckmfitter.in2p3.fr`.

[29] A. Bevan *et al.*, arXiv:1411.7233 [hep-ph]; for updates, see http://www.utfit.org.

[30] K. A. Olive *et al.* [Particle Data Group Collaboration], Chin. Phys. C **38** (2014) 090001 and 2015 update. doi:10.1088/1674-1137/38/9/090001

[31] K. De Bruyn and R. Fleischer, JHEP **1503** (2015) 145 doi:10.1007/JHEP03(2015)145 [arXiv:1412.6834 [hep-ph]].

[32] M. Ciuchini, E. Franco, S. Mishima and L. Silvestrini, JHEP **1210** (2012) 029 doi:10.1007/JHEP10(2012)029 [arXiv:1205.4948 [hep-ph]].

[33] M. Gronau and D. London, Phys. Rev. Lett. **65** (1990) 3381. doi:10.1103/PhysRevLett.65.3381

[34] A. S. Dighe, I. Dunietz, H. J. Lipkin and J. L. Rosner, Phys. Lett. B **369** (1996) 144 doi:10.1016/0370-2693(95)01523-X [hep-ph/9511363].

[35] A. S. Dighe, I. Dunietz and R. Fleischer, Eur. Phys. J. C **6** (1999) 647 doi:10.1007/s100520050372, 10.1007/s100529800954 [hep-ph/9804253].

[36] R. Fleischer and R. Knegjens, Eur. Phys. J. C **71** (2011) 1789 doi:10.1140/epjc/s10052-011-1789-9 [arXiv:1109.5115 [hep-ph]].

[37] L. Bel, K. De Bruyn, R. Fleischer, M. Mulder and N. Tuning, JHEP **1507** (2015) 108 doi:10.1007/JHEP07(2015)108 [arXiv:1505.01361 [hep-ph]].

[38] J. D. Bjorken, Nucl. Phys. Proc. Suppl. **11** (1989) 325. doi:10.1016/0920-5632(89)90019-4

[39] D. Bortoletto and S. Stone, Phys. Rev. Lett. **65** (1990) 2951. doi:10.1103/PhysRevLett.65.2951

[40] J. L. Rosner, Phys. Rev. D **42** (1990) 3732. doi:10.1103/PhysRevD.42.3732

[41] M. Neubert and B. Stech, Adv. Ser. Direct. High Energy Phys. **15** (1998) 294 doi:10.1142/9789812812667_ 0004 [hep-ph/9705292].

[42] M. Beneke, G. Buchalla, M. Neubert and C. T. Sachrajda, Phys. Rev. Lett. **83** (1999) 1914 doi:10.1103/PhysRevLett.83.1914 [hep-ph/9905312];

[43] M. Beneke, G. Buchalla, M. Neubert and C. T. Sachrajda, Nucl. Phys. B **606** (2001) 245 doi:10.1016/S0550-3213(01)00251-6 [hep-ph/0104110].

[44] M. Beneke, T. Huber and X. Q. Li, Nucl. Phys. B **832** (2010) 109 doi:10.1016/j.nuclphysb.2010.02.002 [arXiv:0911.3655 [hep-ph]].

[45] R. Fleischer, N. Serra and N. Tuning, Phys. Rev. D **83** (2011) 014017 doi:10.1103/PhysRevD.83.014017 [arXiv:1012.2784 [hep-ph]].

[46] J. A. Bailey *et al.* [Fermilab Lattice and MILC Collaborations], Phys. Rev. D **92** (2015) no. 1, 014024 doi:10.1103/PhysRevD.92.014024 [arXiv:1503.07839 [hep-lat]].

[47] D. Du, A. X. El-Khadra, S. Gottlieb, A. S. Kronfeld, J. Laiho, E. Lunghi, R. S. Van de Water and R. Zhou, Phys. Rev. D **93** (2016) no. 3, 034005 doi:10.1103/PhysRevD.93.034005 [arXiv:1510.02349 [hep-ph]].

[48] M. Ciuchini, E. Franco, G. Martinelli, M. Pierini and L. Silvestrini, Phys. Lett. B **515** (2001) 33 doi:10.1016/S0370-2693(01)00700-6 [hep-ph/0104126].

[49] R. Aaij *et al.* [LHCb Collaboration], arXiv:1610.08288 [hep-ex].

[50] A. Sibidanov *et al.* [Belle Collaboration], Phys. Rev. D **88** (2013) 032005 doi:10.1103/PhysRevD.88.032005 [arXiv:1306.2781 [hep-ex]].

[51] J. P. Lees *et al.* [BaBar Collaboration], Phys. Rev. D **86** (2012) 092004 doi:10.1103/PhysRevD.86.092004 [arXiv:1208.1253 [hep-ex]].

[52] I. Sentitemsu Imsong, A. Khodjamirian, T. Mannel and D. van Dyk, JHEP **1502** (2015) 126 doi:10.1007/JHEP02(2015)126 [arXiv:1409.7816 [hep-ph]].

[53] P. Ball, Phys. Lett. B **644** (2007) 38 doi:10.1016/j.physletb.2006.11.034 [hep-ph/0611108].

[54] R. Fleischer, N. Serra and N. Tuning, Phys. Rev. D **82** (2010) 034038 doi:10.1103/PhysRevD.82.034038 [arXiv:1004.3982 [hep-ph]].

[55] LHCb Collaboration, preliminary, talk given by S. Perazzini at CKM 2016, Mumbai, India, LHCb-CONF-2016-018.

[56] A. J. Buras and R. Fleischer, Phys. Lett. B **341** (1995) 379 doi:10.1016/0370-2693(95)80018-S, 10.1016/0370-2693(94)01314-3 [hep-ph/9409244].

[57] M. Gronau and J. L. Rosner, Phys. Lett. B **482** (2000) 71 doi:10.1016/S0370-2693(00)00508-6 [hep-ph/0003119].

[58] R. Fleischer, Phys. Rev. D **60** (1999) 073008 doi:10.1103/PhysRevD.60.073008 [hep-ph/9903540].

[59] S. Descotes-Genon, J. Matias and J. Virto, Phys. Rev. Lett. **97** (2006) 061801 doi:10.1103/PhysRevLett.97.061801 [hep-ph/0603239].

[60] R. Fleischer and S. Recksiegel, Eur. Phys. J. C **38** (2004) 251 doi:10.1140/epjc/s2004-02023-0 [hep-ph/0408016].

[61] B. Aubert *et al.* [BaBar Collaboration], Phys. Rev. Lett. **97** (2006) 171805 doi:10.1103/PhysRevLett.97.171805 [hep-ex/0608036].

[62] Y. Nakahama *et al.* [Belle Collaboration], Phys. Rev. Lett. **100** (2008) 121601 doi:10.1103/PhysRevLett.100.121601 [arXiv:0712.4234 [hep-ex]].

[63] B. Pal *et al.* [Belle Collaboration], Phys. Rev. Lett. **116** (2016) no. 16, 161801 doi:10.1103/PhysRevLett.116.161801 [arXiv:1512.02145 [hep-ex]].